Final Report for Grant Activities No. 582-23-43887-030

Ozone-NO_x-VOC Sensitivity in Texas Urban Areas

Category III, Research Model Development or Application

Final Report

June 24, 2024

PGA No. 582-23-43887-030

Grant Number: 582-18-81339

Tracking Number: 2023-13

Prepared for the Texas Commission on Environmental Quality (TCEQ)

Principal Investigators
Yuxuan Wang, University of Houston

Contributors
Tabitha Lee, University of Houston
Geoffery Roberts, University of Houston
Shailaja Wasti, University of Houston
Xueying Liu, University of Houston

Executive Summary

Surface-level ozone (O_3) is associated with negative health risks which could lead to cardiovascular and respiratory diseases. As such O_3 is a criteria pollutant defined by the EPA and is regulated nationally and on a state-level, to protect the air we breathe. The Texas Commission of Environmental Quality (TCEQ) monitors O_3 across the state of Texas. It is of most importance as urban areas across the state of Texas are in nonattainment, where the EPA standard for acceptable observed ozone concentrations is not met. Surface-level zone is produced through photochemical reactions involving nitrogen oxides (NO_x=NO+NO_2) and volatile organic compounds (VOCs). Ozone formation can be categorized into regimes given the availability of its precursors, such as NO_x-limited, VOC-limited, or transitional. Precursor variability varies spatially and temporally depending on what chemical and meteorological conditions are affecting the urban area. Identifying what regime an urban area is categorized as can lead to effective emission control strategies to help reduce driving precursor emissions of tropospheric ozone and allow for attainment to be achieved across the state of Texas.

We utilize observations of NO_2, a proxy for NO_x emissions, and formaldehyde (HCHO), a proxy for VOC emissions, from routine in situ sampling at ground-level stations, satellite instruments, and photochemical model simulations to understand the spatial and temporal variability of ozone regimes across the state of Texas when the region is met with varying chemical and meteorological conditions. The 2022 ozone season is analyzed specifically under different conditions such as ozone exceedances, weekday, weekends, temperatures greater than the 85th percentile, and others. Regime placement can be determined by indicator ratios, such as the formaldehyde (HCHO) to nitrogen dioxide (NO_2) ratio (hereafter FNR, HCHO:NO_2, or HCHO/NO_2), L_N/Q, or the Sillman indicator. We focus on the ratios of HCHO/NO_2 and L_N/Q. Given the observational constraints with the indicator ratio L_N/Q, this product was simulated using the CAMx photochemical model only. Urban areas in Texas were placed into regimes using L_N/Q for the full ozone season in 2022. The spatially comprehensive regime for each urban area of interest is NO_x-limited for El Paso, Houston, San Antonio, and Dallas when using the L_N/Q ozone production indicator, with areas in the main urban core experiencing a VOC-Limited regime.

The HCHO/NO_2 ratio has been widely applied with numeric regime thresholds in order to place an airshed into a regime as seen in Jin et al. (2020). Using the existing methodology from Jin et al., we find updated regime thresholds in different conditions for four urban areas across Texas: Houston, Dallas, San Antonio, and El Paso. Using TROPOMI and CAMx results, we find that the HCHO/NO_2 ratio varies in different conditions such as the full ozone season and exceedances, and thus its regime threshold changes as well. These findings are consistent across each urban area in Texas allowing one to observe that the HCHO/NO_2 values are not static and depends on the chemical makeup of an airshed, its meteorological conditions and location, as well as the data set in which the HCHO/NO_2 ratio was calculated from. Although variability is observed in the FNR, we see that for the full ozone season in 2022 the dominant regime varies spatially when derived from FNR calculations observed across all observational products, with areas near the urban core seeing VOC-limited or transitional regimes while the suburb and surrounding areas experience a NO_x-limited regime for El Paso, Houston, San Antinio, and Dallas. We note there is a high level of uncertainty associated with the updated regime thresholds calculated in this report and caution should be had when applying these static values to an urban area. Yet, we see consistency with CAMx derived L_N/Q results placing confidence in our methods to categorize the ozone formation regime across the state of Texas when using observational platforms, and photochemical model simulations.

Table of Contents

1: Introduction

The sensitivity of ozone (O_3) to nitrogen oxides (NO_X: $NO+NO_2$) and volatile organic compounds (VOCs) is a critical issue for pollution control policy. For policy measures, the United States Environmental Protection Agency (U.S. EPA) set an updated ozone National Ambient Air Quality Standard (NAAQS) to 70 parts per billion (ppb) in 2015. Areas that adhere to this standard are considered in attainment, while those that exceed this standard are in nonattainment. Across the state of Texas, nonattainment is found, as the 3-year average of the annual fourth-highest daily maximum 8-hr average O_3 concentration measured at ground-level stations (hereafter design value) exceeds the NAAQS standard (design value > 70 ppb). Texas urban areas, including San Antonio, Houston, Dallas-Fort Worth, and El Paso, are of interest due to their potential or current nonattainment status. Their ozone formation is controlled by the nonlinear relationship between NO_x and VOCs concentrations observed in each area. To understand the drivers of ozone production, an air shed is characterized by its sensitivity of ozone formation to NO_x and VOCs and placed into three main regimes: VOC-limited (O_3 production rates are limited by VOCs), NO_x-limited (O_3 production rates are limited by NO_x), and transitional (not strongly limited by VOCs or NO_x). A commonly used method of regime placement is determined by the formaldehyde (HCHO) to nitrogen dioxide (NO_2) ratio (hereafter FNR, HCHO:NO_2, or HCHO/NO_2), as indicated by several studies (Souri et al., 2023, Goldberg et al., 2022, Duncan et al., 2010; Jin et al., 2020, 2017; Jin & Holloway, 2015; Martin et al., 2004). The FNR is considered an ozone formation regime indicator and uses HCHO concentration as a proxy for VOC reactivity (Souri et al., 2020). The predictive power of the FNR can be used to tease out drivers of ozone formation through its precursors and illustrate how regimes change spatially and temporally when met with specific chemical and meteorological conditions. Additionally, other ozone indicator ratios such as the Sillman indicator ratio of hydrogen peroxide to nitric acid (H_2O_2/HNO_3), or the fraction of radicals (Q) lost to NO_x reactions (L_N) presented as L_N/Q can describe an airshed's ozone formation regime. The Sillman and L_N/Q indicators are quite robust, but see limited use compared to the FNR due to observational constraints. To overcome constraints, photochemical models can be employed to simulate the chemical species required and the use of the Sillman and L_N/Q indicator ratios can be compared to that of the FNR to observe how the different ratios categorize and describe an airshed when it experiences specific meteorological or chemical conditions driving ozone production.

Observations of NO_2 and HCHO can be gathered from routine in situ sampling at ground-level stations, satellite instruments, and photochemical model simulations. In this study, all three platforms will be employed and intercompared. Specifically, surface observations from regulatory monitors maintained by the Texas Commission on Environmental Quality (TCEQ), satellite observations from the TROPOspheric Monitoring Instrument (TROPOMI; Veefkind et al., 2012), and photochemical model simulations by the Comprehensive Air Quality Model with Extensions (CAMx), the regulatory photochemical model used by the TCEQ will be analyzed throughout the ozone seasons of 2019 to 2023, except for the CAMx simulation which covered only the 2022 ozone season. In this project utilizing the observations of the April – October ozone seasons available (i.e., up to October 2023), the focus will be on the power of satellite observations, in situ monitors, and photochemical models to observe and categorize the VOC (inferred using HCHO) and NO_x (inferred using NO_2) sensitivity of ozone formation in Texas urban areas through two ozone regime indicators: the FNR and L_N/Q. The evaluation of NO_2 and HCHO datasets from different platforms such as in situ sampling at ground-level stations, satellite instruments, and photochemical model simulations will provide a better understanding on the uncertainties associated with ozone production and the regime in which an airshed can be categorized.

We utilize TROPOMI observations and the CAMx model to evaluate the ozone regime classifications in four urban areas of Texas: Houston, Dallas, San Antonio, and El Paso. We examine the differences in TROPOMI when it is physically oversampled, regridded, and updated with CAMx a priori information as well as CAMx results on the FNR. Then, we place FNR values into regimes in which it is following definitions from Jin et al., 2020 and internally derived regimes following similar methodology.

Following these results, we offer recommendations on ozone regime thresholds for the urban areas which could be used to constrain emissions and help Texas urban areas achieve attainment status.

2: Conditions

Different time periods and conditions to test the FNR across urban areas in Texas were defined. Counties of interest are Harris County for Houston, Bexar County for San Antonio, El Paso County for El Paso, and Tarrant and Dallas County for Dallas. Satellite observations were split yearly (i.e., 2019, 2020, 2021, 2022, 2023), seasonally (i.e., spring (April - May), summer (June – August), and fall (September - October)), by month (i.e., April – October), and with different conditions applied. The delineation of periods and conditions will allow one to observe how the FNR changes in different periods, over time, and test the limits of satellite observations resolving the FNR in Texas urban areas with varying numbers of observations. Conditions defined include but are not limited to: (1) weekday (Tuesday - Friday) and weekend (Saturday - Sunday) following definitions from Jin et al. (2020), Psuede et al. (2012), and Demetillo et al. (2020), and (2) ozone exceedances where the daily eight-hour ozone concentration meets or exceeds 71 ppbv following https://www.tceq.texas.gov/cgi-bin/compliance/monops/8hr_exceed.pl.

High-Resolution Rapid Refresh (HRRR) is a weather model that assimilates radars' data every 15 minutes over a 1-hour period. HRRR can provide hourly updated, cloud-resolving, convection-allowing meteorology information. HRRR observations with a given resolution of 3 km x 3 km were interpolated to the same resolution of TROPOMI (0.01° x 0.01°) and selected to match the time of TROPOMI overpass (13:30 Local Time) and counties of interest. HRRR results allowed for the identification of days with specific meteorology conditions such as (3) temperatures greater than the 85^{th} and 95^{th} percentile of each location, and (4) specific wind directions. Interpolated temperature grids from HRRR corresponding to the TROPOMI oversampled resolution (0.01° x 0.01°) and within each county of interest were averaged daily. Percentiles were then calculated on a monthly basis throughout the ozone season (April – October) based on the daily mean values for each region. Days exhibiting a value equal or greater than the 85^{th} or 95^{th} percentile were considered as a day of interest in this study. The percentiles varied for each county and were as such for Texas 31.12 and 31.87 °C, Houston 28.4 and 28.71 °C, San Antonio 28.54 and 28.84 °C, Dallas 29.36 and 30.0 °C, El Paso 32.97 and 34.04 °C, respectively for the 85^{th} and 95^{th} percentiles. Winds were divided into northerly (303.75° – 56.25°), southernly (123.75° – 236.25°), westerly (236.25° - 303.75°), and easterly (56.25° – 123.75°) directions and each division was analyzed for its impact on the FNR value. We chose temperature and winds as simple but key meteorological factors to define meteorological conditions because previous studies have demonstrated their importance as meteorological drivers of ozone air quality variability in Texas (Bernier et al., 2019; Li et al., 2020).

Figure 1 displays the total relative days of different conditions defined for each county of interest and **Figure 2** displays the days for which the design value exceeded the NAAQS standard within each defined condition. Separated by urban area, one can see key features driving exceedances, such as westward winds or temperatures greater than the 85^{th} percentile in El Paso, or eastward winds in Dallas and Houston.

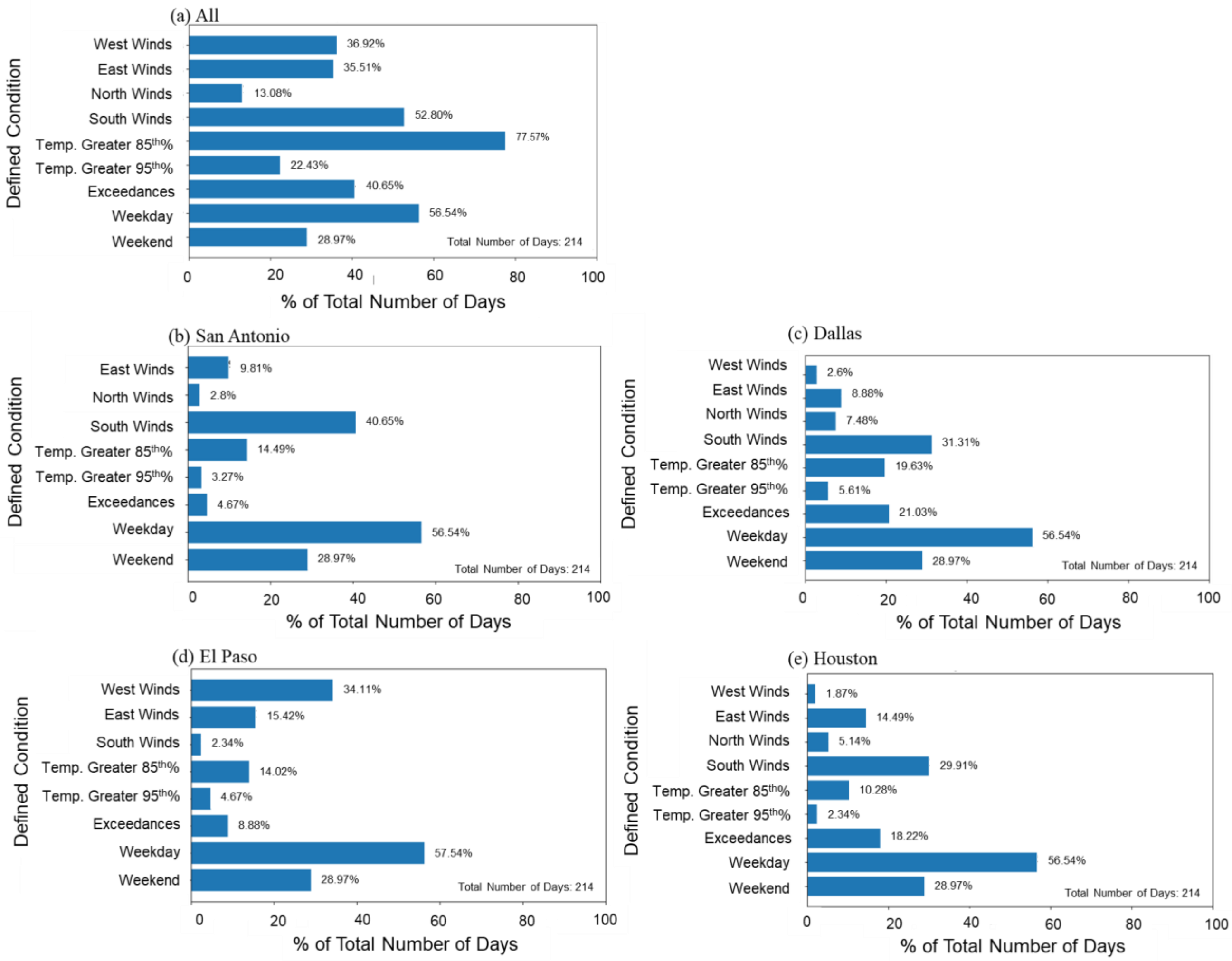

Figure 1. Relative percent of days within the Texas ozone season (April – October) for each defined condition from April – October 2022, totaling 214 days, for all of Texas in (a) and each county of interest being Bexar County for (b) San Antonio, Tarrant, and Dallas County for (c) Dallas, El Paso County for (d) El Paso, and Harris County for (e) Houston.

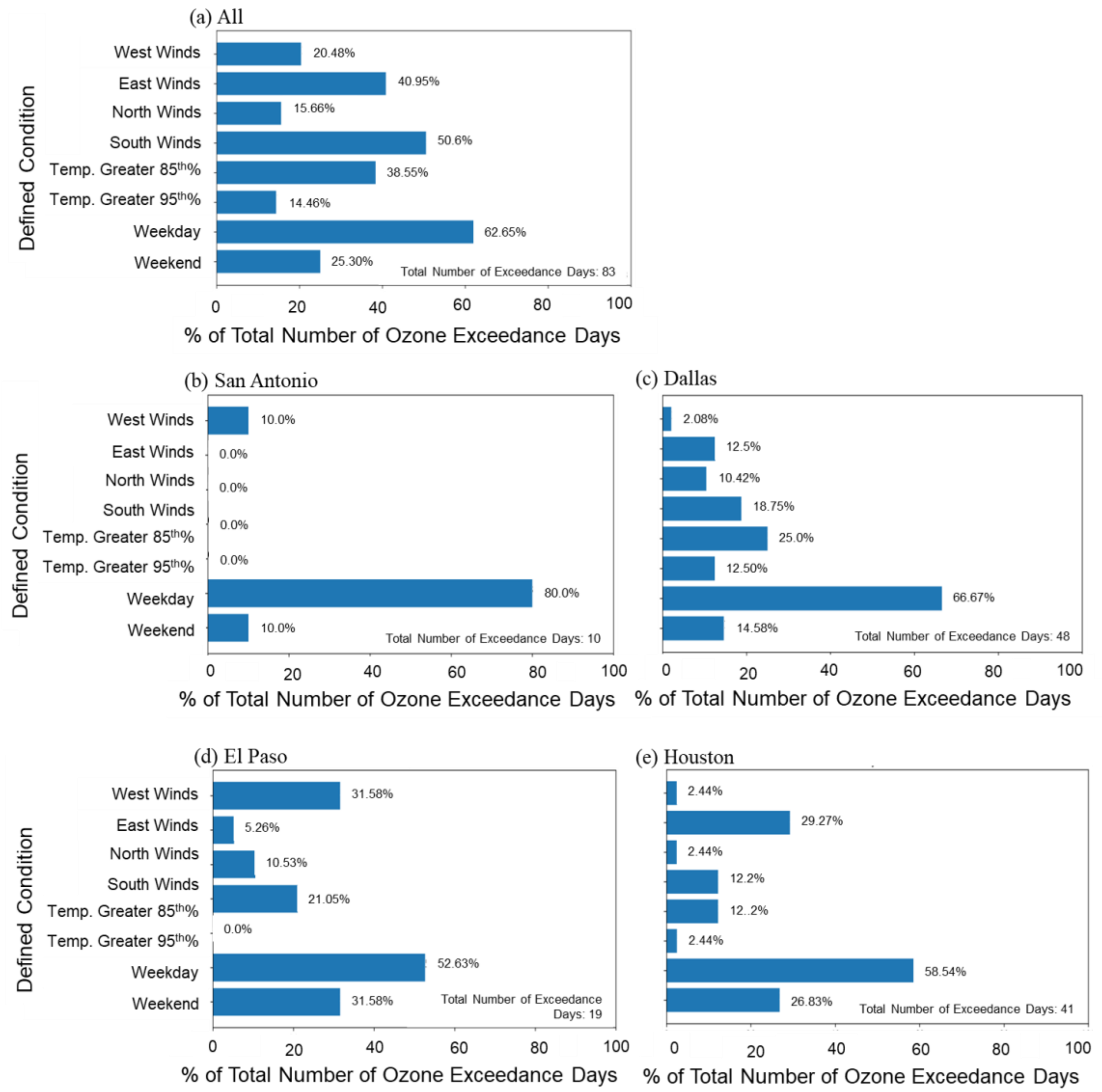

Figure 2. Relative percent of ozone exceedance days defined by (https://www.tceq.texas.gov/cgi-bin/compliance/monops/8hr_exceed.pl) within the Texas ozone season (April – October) for each defined condition from April – October 2022, totaling 83 days, for all of Texas in (a) and each county of interest being Bexar County for (b) San Antonio, Tarrant, and Dallas County for (c) Dallas, El Paso County for (d) El Paso, and Harris County for (e) Houston.

3: Intercomparison Products

3.1: CAMx

In this project period, we use a 4 x 4 km^2 CAMx simulation, version 7.10. CAMx is a photochemical model which solves the 3-dimensional Eulerian continuity equation based on the "one-atmosphere" framework for different chemical species in a defined domain (Soleimanian et al., 2023). It is a regulatory model employed by the TCEQ to simulate pollutants and their sensitivities to pollution control policies. To simulate each Texas urban area, a 12 km^2 CAMx simulation was constructed and then nested down to two 4 km^2 domains were centered over El Paso and east Texas encompassing the urban centers of Houston, Dallas, and San Antonio as shown in **Figure 3**. The CAMx simulation for the 2022 ozone season (April – October) was driven offline by the Weather Research Forecast (WRF) model (version 3.9.1.1). The WRF model configuration followed Soleimanian et al. (2023), where the local closure Mellor-Yamada-Nakanishi-Niino (MYNN) planetary boundary layer (PBL) scheme (Nakanishi and Niino, 2009), Morrison double moment (2 M) micro-physics scheme (Morrison et al., 2009), Rapid Radiative Transfer Model (RRTMG) longwave and shortwave radiation schemes (Iacono et al., 2008), Monin-Obukhov similarity surface layer scheme (Chen et al., 1997), Noah land-surface module (Chen and Dudhia, 2001), and the New Tiedtke cumulus parameterization for sub-grid-scale effects of clouds (Tiedtke, 1989; Zhang et al., 2011) were set. The initial and meteorological boundary conditions were from HRRR with hourly temporal resolution. All domains had 45 vertical levels in the native WRF model grid extending from the surface to the 50 hPa pressure level. The WRF vertical layers were mapped to 30 CAMx vertical layers using the WRF-CAMx version 5.1 pre-processor tool. The WRF layers were compressed into 30 unevenly distributed levels with higher resolution near the surface that extend up to ~11km (100 hPa) above ground level. Anthropogenic emissions data from the 2019 State Implementation Plan (SIP) modeling platform provided by TCEQ was converted and used in the model (as discussed in Li et al. (2023)). Biogenic emissions are generated from the Biogenic Emission Inventory System (BEIS) and wildfire emissions are based on the Fire Inventory from NCAR (FINNv2), and ship emissions estimated from the Gulfwide Emissions Inventory (GWEI). No lighting emissions are included in the model.

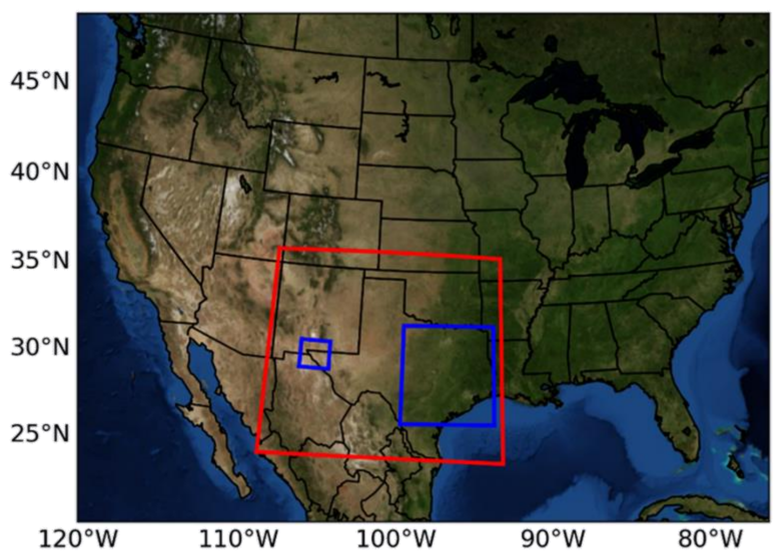

Figure 3. CAMx 12km (red), and 4km (blue) domains for Texas urban areas.

The initial and boundary conditions for the 4km domains were obtained from a global simulation of the GEOS-Chem (version 14.1.1) model. Emission in GEOS-Chem is from National Emissions Inventory (NEI) 2011 NO_x emissions scaled down to 2022. The CAMx simulation was generated with a 10-day spin-up period and only the vertical layers matching the TROPOMI tropospheric vertical column were analyzed to investigate if regimes can be delineated across the state of Texas for different meteorological and chemical conditions.

CAMx simulated NO_2 and O_3 sampled at TROPOMI overpass (13:30 LT) were evaluated against surface concentrations from the TCEQ-maintained Texas Air Monitoring Information System (TAMIS), further described in Section 3.3. The four counties of interest, Harris County for Houston, Bexar County for San Antonio, El Paso County for El Paso, and Tarrant and Dallas County for Dallas, were evaluated. We acknowledge that NO_2 in situ monitors have limitations, yet we compare only monitored NO_2 to

CAMx NO_2, and do not consider other components of NO_x or NOy. Routinely measured O_3 is compared to CAMx O_3 corresponding to the time of the TROPOMI overpass.

Figure 4 and **5** shows the NO_2 and O_3 performance, respectively. Observed NO_2 is not simulated well by CAMx, which is typical for this model at the 4km grid resolution (Goldberg et al., 2022) due to the model inability of resolving point and traffic emissions and exclusion of some NO_x sources (e.g. lightning). **Figure 6** shows CAMx-simulated 2022 ozone season mean NO_2 with in situ observation overlaid, with each dataset sampled at TROPOMI overpass (13:30 LT) as stated above. In this figure, we observe that CAMx does well in simulating the spatial patterns of ambient NO_2 concentrations, but again struggles to capture gradients observed within county limits. Comparatively, CAMx performance improves when simulating O_3 as shown in **Figure 5**. High R^2 values and low mean biases are observed for all four counties, and notably Houston and Dallas, with R^2 of 0.78 (Houston) and 0.75 (Dallas), and mean basis of 2.66 ppbv (Houston) and 1.40 ppbv (Dallas) respectively. Since ozone is secondary pollutant with a large regional influence, high agreement between CAMx simulated ozone and observations is likely due to the CAMx model well reproducing local- and region-scale ozone chemistry and transport. Note the good agreement shown in **Figure 5** pertains to only 13:30 LT and may not be generalized to other time periods. For example, photochemical models are known to have issues in simulating nighttime ozone. **Figure 7** shows CAMx-simulated 2022 ozone season mean O_3 with in situ observation overlaid, with each dataset sampled at TROPOMI overpass (13:30 LT). It further illustrates the greater agreement of CAMx simulated O_3 with observations, but still confirms the difficulty the model has in simulating sharp gradients of O_3 concentrations within a city center.

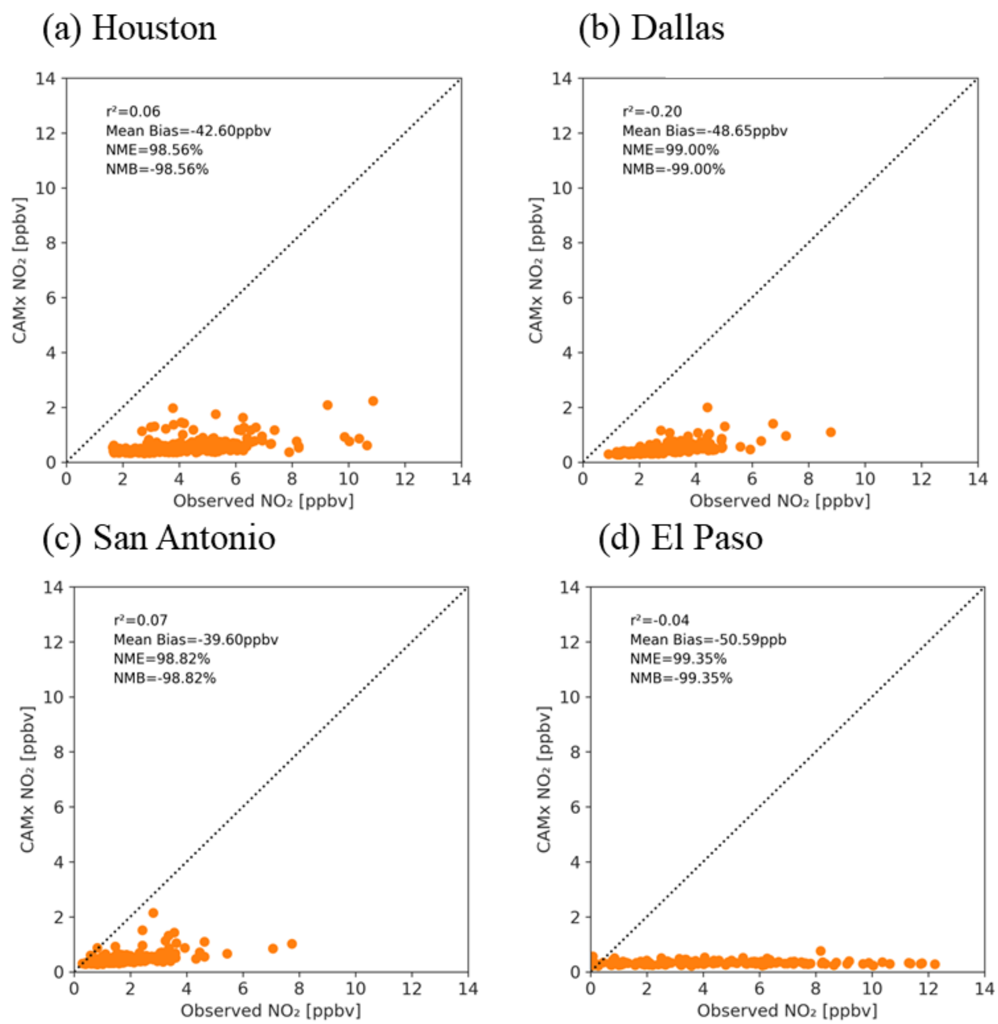

Figure 4. CAMx model performance for NO_2 for overpass 13:30 LT (local time). Simulated model NO_2 is compared to the TCEQ-maintained Texas Air Monitoring Information System (TAMIS) for the four counties of interest, (a) Harris County for Houston, (b) Tarrant and Dallas County for Dallas, (c), Bexar County for San Antonio, and (d) El Paso County for El Paso.

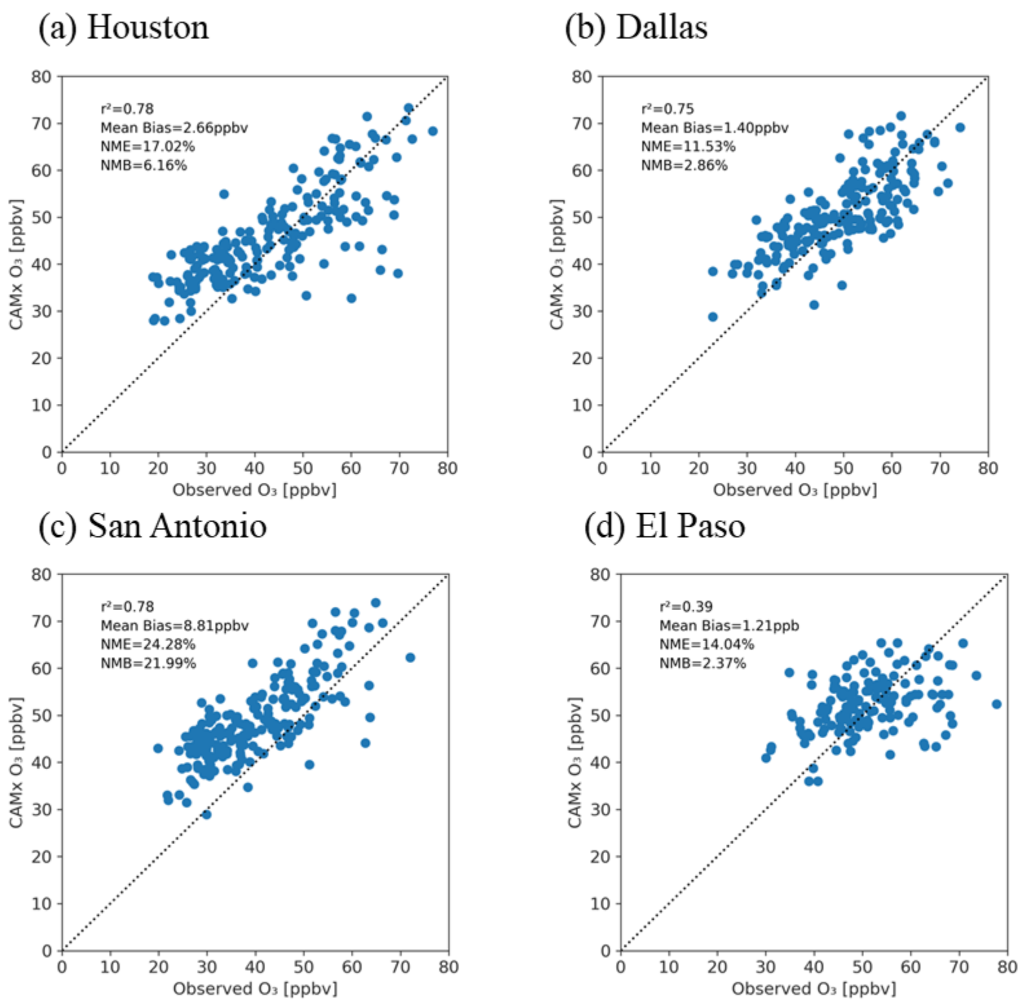

Figure 5. CAMx model performance for O_3 for overpass 13:30 LT (local time). Simulated model O_3 is compared to the TCEQ-maintained Texas Air Monitoring Information System (TAMIS) for the four counties of interest (a) Harris County for Houston, (b) Tarrant and Dallas County for Dallas, (c), Bexar County for San Antonio, and (d) El Paso County for El Paso.

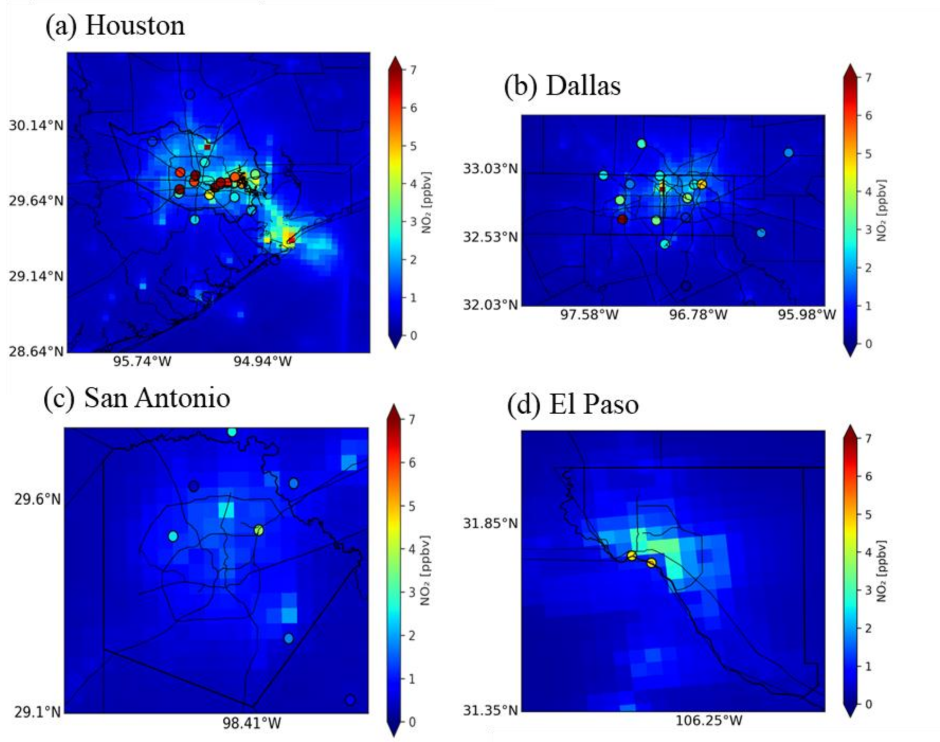

Figure 6. CAMx NO_2 spatial performance of the total 2022 ozone season (April – October) for overpass 13:30 LT (local time). Simulated model NO_2 is underlaid the TCEQ-maintained Texas Air Monitoring Information System (TAMIS) for the four counties of interest. (a) Harris County for Houston, (b) Tarrant and Dallas County for Dallas, (c), Bexar County for San Antonio, and (d) El Paso County for El Paso.

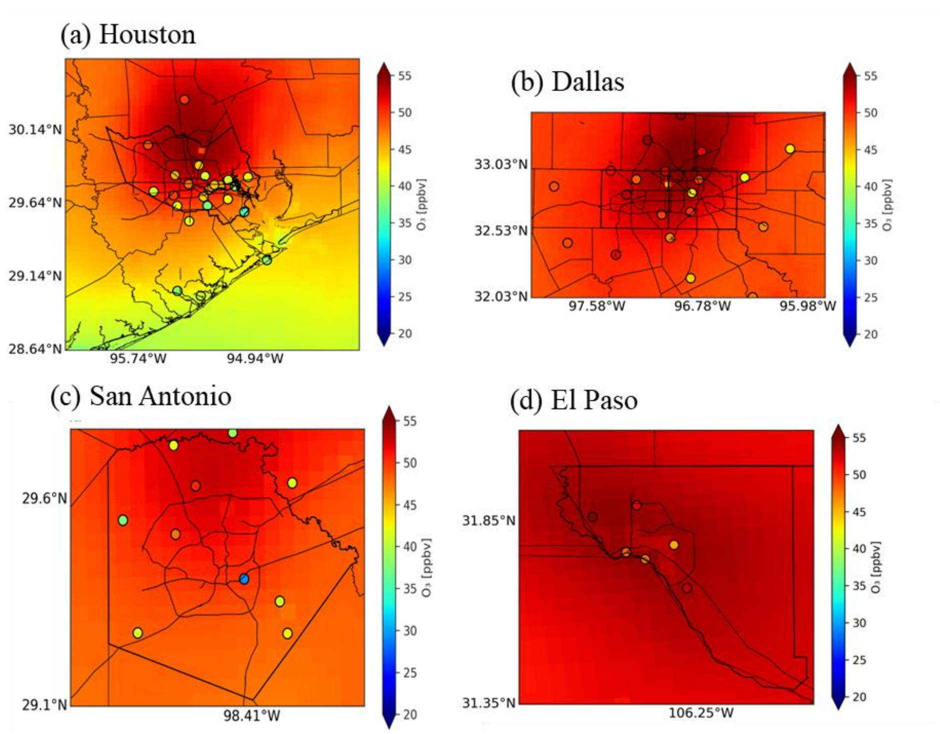

Figure 7. CAMx O_3 spatial performance of the total 2022 ozone season (April – October) for overpass 13:30 LT (local time). Simulated model O_3 is underlaid the TCEQ-maintained Texas Air Monitoring

Information System (TAMIS) for the four counties of interest. (a) Harris County for Houston, (b) Tarrant and Dallas County for Dallas, (c), Bexar County for San Antonio, and (d) El Paso County for El Paso.

3.2: TROPOMI

Satellite instruments have been used to continuously detect changes in atmospheric NO_2, HCHO, and other trace gases since the 1990s, notably with polar-orbiting satellite missions such as Global Ozone Monitoring Experiment (GOME; Burrows et al., 1999), Global Ozone Monitoring Experiment 2 (GOME-2; Munro et al., 2016), SCanning Imaging Absorption spectroMeter for Atmospheric CartograpHY (SCIAMACHY; Bovensmann et al., 1999), Ozone Monitoring Instrument (OMI; Levelt et al., 2006), and TROPOspheric Monitoring Instrument (TROPOMI; Veefkind et al., 2012). These polar-orbiting instruments have been building off one another, improving aspects such as detection techniques and spatial resolution. Being one of the newest polar-orbiting instruments, TROPOMI carries an initial spatial resolution of 3.5×7 km^2, and since 6 August 2019, 3.5×5.6 km^2 at nadir, which is a great improvement in spatial resolution compared to that of GOME (40×320 km^2), GOME-2 (40×80 km^2), SCIAMACHY (30×60 km^2), and OMI (13×24 km^2). The high spatial resolution of TROPOMI products makes it possible to observe fine-scale changes in ozone precursor emissions, which reveals more information on the spatial distribution of local O_3 formation chemistry. As such, to test the ability of the predictive power of the FNR using satellite observations, we employ TROPOMI observations. TROPOMI is aboard the Sentinel 5 Precursor (S5P). The sun-synchronous instrument uses passive remote sensing to observe gases down into the troposphere and gives near-global coverage in one day with an equator crossing time near 13:30 local solar time.

Improvements to the signal-to-noise ratio and spatial resolution in the TROPOMI instrument have allowed for quality conclusions using short temporal periods for NO_2 observations (Lee et al., 2022, Goldberg et al., 2019). TROPOMI HCHO observations have found success using short timescales (Alvarado et al., 2020; Theys et al., 2020). HCHO is a weaker UV-visible absorber than NO_2, leading to HCHO columns retrieved from satellite observations being more prone to noise than NO_2 retrievals (Jin et al., 2020). Additionally, given the natural variability of HCHO and pseudo-noise dependent on the spatial and temporal scale, longer averages in HCHO column densities are recommended, see DeSmedt et al. (2021) for further details. In this project section, we test the ability of TROPOMI to resolve O_3 formation chemistry in varying temporal periods, with specific ranges from 7 months to 10 days included in this report.

TROPOMI NO_2 observations utilized a quality filter (qa) greater than 0.75, where this value filters out observations presenting an error flag or a solar zenith angle larger than 80° and a cloud radiance fraction (CRF) at 340 nm larger than 0.3. NO_2 observations prior to 2022-07-26 are reprocessed (RPRO) v2.04.0, while those that fall between 2022-07-26 to 2023-03-11 are offline (OFFL) v2.04.0, observations from 2023-03-12 and forward are OFFL v2.05.0. TROPOMI HCHO v2.04+ observations available for April – October 2019 – 2023 were oversampled to a 0.01° resolution using filtering criteria from DeSmedt et al. (2021) where the quality filter (qa) was greater than 0.5 which filters out observation with an error flag or a solar zenith angle larger than 70°, a cloud radiance fraction (CRF) at 340 nm larger than 0.6, air mass factor (AMF) smaller than 0.1, and an activated snow and ice flag. HCHO observations prior to 2022-08-03 are RPRO v2.4.01, while those that fall between 2022-08-26 to 2023-07-15 are OFFL v2.4.01, observations from 2023-07-16 and forward are OFFL v2.05.0. All satellite observations employed in FNR calculations have at least 85% quality pixels in the area of interest.

Here we take three approaches with TROPOMI observations. The three approaches are (1) oversampling following Sun et al., 2018, (2) regridding to match the CAMx domain, and (3) updating TROPOMI observations with a new air mass factor (AMF) derived from CAMx. In the first approach, available TROPOMI NO_2 and HCHO v2.04+ observations for April – October 2019 – 2023 were oversampled to a 0.01° resolution following a physics-based oversampling process from Sun et al., (2018). Rather than assuming satellite observations are points or polygons as done in various oversampling methods, this approach represents each satellite observation as a sensitivity distribution on the ground. The physical oversampling approach is particularly advantageous during short temporal windows and shows significantly improved visualization of trace gas distribution and local gradients (Sun et al., 2018). With the second approach, available TROPOMI NO_2 and HCHO v2.04+ observations for April – October 2022 were regridded to the model resolution creating a new level 3 data product for comparison with model results, listed as TROPOMI in this report. After regridding the TROPOMI observations, the model and satellite products are now horizontally equivalent, yet the satellite a priori employed in the TROPOMI retrieval has different horizontal and vertical resolutions and distributions of O_3 precursors than CAMx. Additional processing is thus required to limit any artificial differences in the comparison of TROPOMI and CAMx. This additional processing is done using two methods: applying the averaging kernel or recalculating the AMF. Here, we recalculate the AMF and is the third approach utilizing TROPOMI observations.

The AMF is a unitless conversion value used to convert the slant column into the vertical column. It is a function of the satellite viewing angles, solar angles, the effective cloud radiance fraction and pressure, the vertical profile share of NO_2 and HCHO provided by a chemical transport model simulation (for operational data, the TM5-MP model is used at 1 × 1° resolution; Williams et al., 2017), and the surface reflectivity (for operational data, climatological Lambertian-equivalent reflectivity is used at a 0.5 × 0.5° resolution; Kleipool et al., 2008) (Goldberg et al., 2022). A more appropriate intercomparison between TROPOMI and CAMx-derived trace gas columns requires the standard AMF found in TROPOMI observations to be updated to a new CAMx-derived AMF. To recalculate the AMF for each TROPOMI pixel, we first calculate the air mass factor for each CAMx model grid cell. The CAMx-AMF is a function of the NO_2 or HCHO shape factor from the model grid cell and the scattering weight from the TROPOMI pixel that overlaps it. The average of the CAMx-AMFs within a TROPOMI pixel is calculated to create a single day-specific tropospheric recalculated AMF for each TROPOMI pixel. The new CAMx-AMF is then used to convert the total slant column from TROPOMI into a tropospheric vertical column following **Equations 1 and 2**, where x_a is the partial NO_2 or HCHO column, and SW is the scattering weights of the optical atmospheric/surface properties. For more information on this procedure, please see Goldberg et al. (2017).

$$VCD_{trop} = \frac{SCD_{total} - SCD_{strat}}{AMF_{trop}} \quad (1) \qquad AMF_{trop} = \frac{\sum_{surface}^{tropopause} SW \times x_a}{\sum_{surface}^{tropopause} x_a} \quad (2)$$

where $AMF_{trop} = \frac{SCD_{trop}}{VCD_{trop}}$

TROPOMI HCHO does not report stratospheric column information so the methodology is adapted to remove stratospheric influences. CAMx outputs were sampled at the local time of the TROPOMI overpass, 13:30 LT, which allows the new vertical column to be directly compared to CAMx-independent TROPOMI observations as well as any tropospheric vertical columns from the CAMx model simulation. **Figure 8** and **9** compare a selection of the data products used in this project, while **Figure 10** shows the correlation between the TROPOMI products and CAMx.

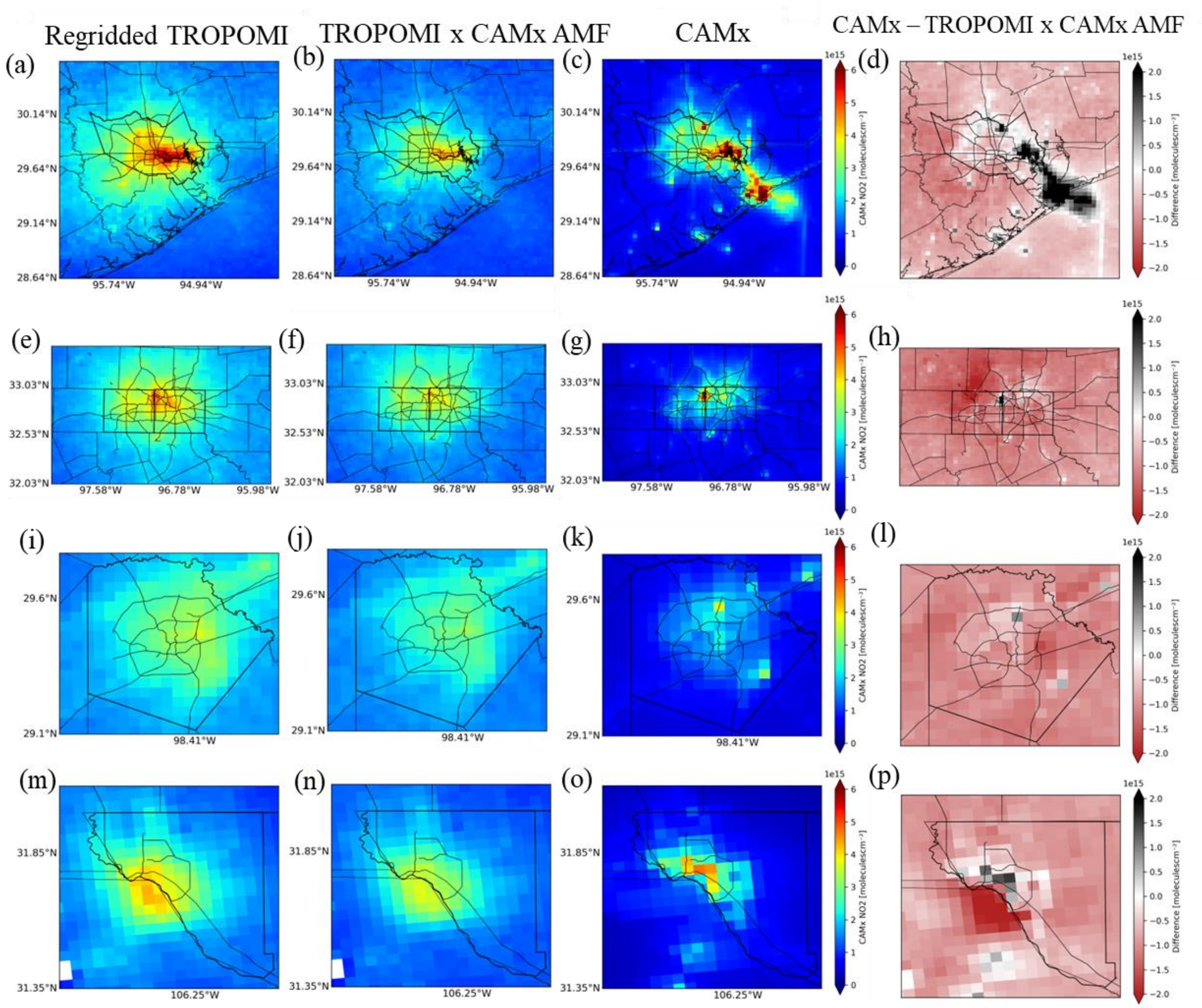

Figure 8. Intercomparison products used in this study shown for the NO_2 tropospheric vertical column averaged across the 2022 ozone season, defined as April – October for each urban area of interest for Texas. (a.e,i,m) TROPOMI NO_2 processor version 2.04, (b,f,j,n) TROPOMI observations updated with the CAMx AMF, (c,g,k,o) CAMx, (d,h,l,p) the difference between CAMx simulated NO_2 and the updated TROPOMI x CAMx AMF NO_2.

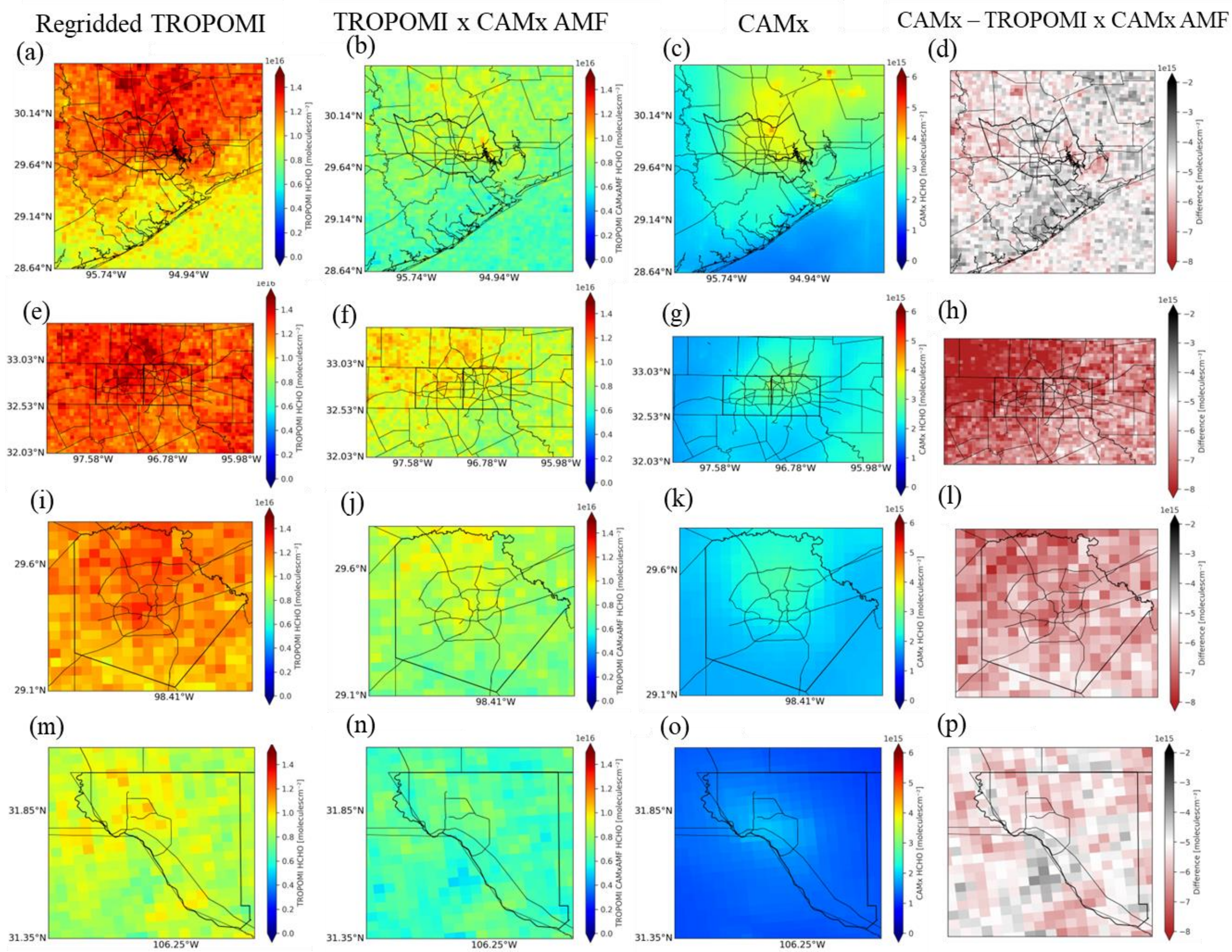

Figure 9. Intercomparison products used in this study shown for the HCHO tropospheric vertical column averaged across the 2022 ozone season, defined as April – October for each urban area of interest for Texas. (a,e,i,m) TROPOMI HCHO processor version 2.04, (b,g,j,n) TROPOMI observations updated with the CAMx AMF, (c,g,k,o) CAMx, (d,h,l,p) the difference between CAMx simulated HCHO and the updated TROPOMI x CAMx AMF HCHO. Note the differing scale for CAMx (c,g,k,o)

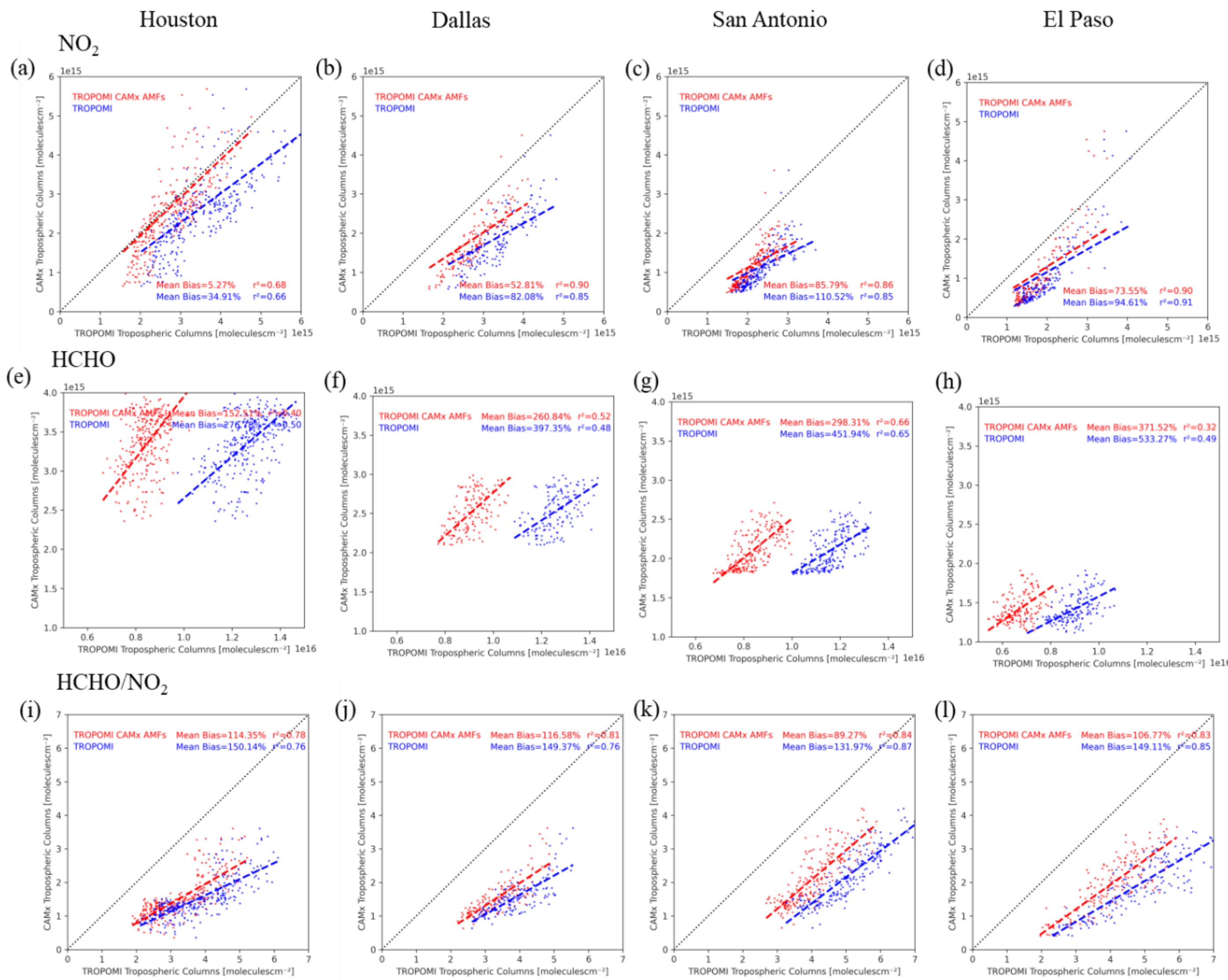

Figure 10. Correlation of TROPOMI-based products and CAMx for each urban area being Houston (a, e, i), Dallas (b, f, j), San Antonio (c, g, k), El Paso (d, h, l). NO_2 correlation is shown in a-d, HCHO in e-h and HCHO/NO2 in i-l. 1:1 line (black dashed) is shown when available. The correlation of TROPOMI with CAMx AMFs are shown in red and regridded TROPOMI is shown in blue.

3.3: In Situ Observations

In-situ stationary surface observations were obtained from the TAMIS, which is an online database of archived surface observational data for the Texas region. Nitrogen dioxide and ozone concentrations are measured every 5 minutes using the continuous monitoring equipment (autonomous) in the stations and are given in ppb. We averaged each hour, requiring a minimum of 45 minutes of data to be present, to give the hourly average. Formaldehyde is measured by a carbonyl sampler (canister sample) and is normally collected every 6 days and analyzed using high-performance liquid chromatography. Values are given in ppb and sample duration is usually 24-hours. Some sites had three 8-hour samples every 3rd day for the months of June through August. Available surface observation station data for April - October 2019 - 2023 was collected from TAMIS. The species ozone, nitrogen dioxide, and formaldehyde were pulled for the regions of Houston, DFW, San Antonio, and El Paso. **Figure 11** displays the location of the 74 monitoring stations which had available data for the 4 regions, with 28 stations located in Houston, 22 stations located in DFW, 16 stations located in San Antonio, and 8 stations located in El Paso.

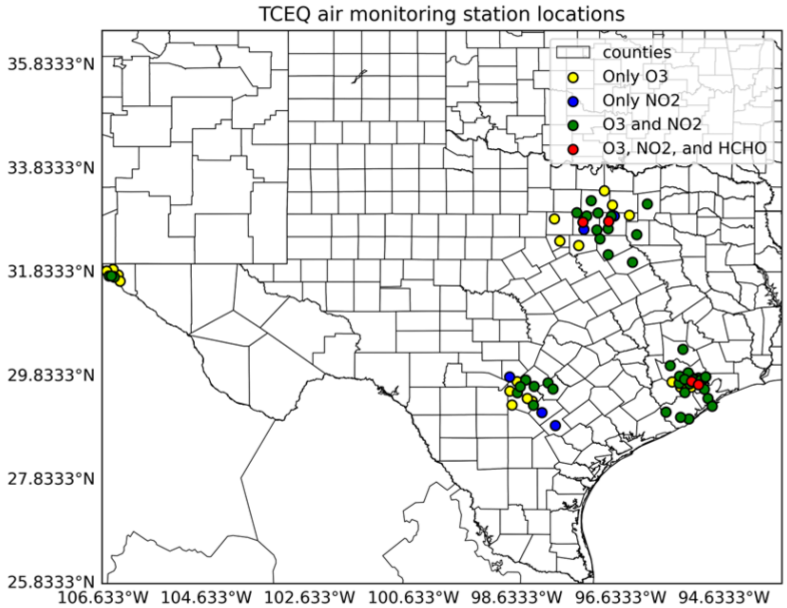

Figure 11. Locations of the TCEQ air monitoring stations for the cities of El Paso (far left), San Antonio (middle left), Dallas/Fort Worth (middle right) and Houston (far right). A yellow circle represents a station that only had O_3 data, blue circle represents a station that only had NO_2 data, green circle represents a station that had both O_3 and NO_2 data, and a red circle represents a station that had Formaldehyde, O_3, and NO_2 data.

Data was collected from a total of 74 sites for the 4 regions. For the Houston region, a total of 28 sites had data of which 26 sites had data for ozone, 23 stations had data for nitrogen dioxide, a total of 21 stations had data for both ozone and nitrogen dioxide, and a total of 2 sites had data for formaldehyde. One of the stations, Deer Park #2, had both 8-hour and 24-hour data while the other station, Clinton, only had 24-hour data. For the DFW region, a total of 22 stations had data of which 20 stations had data for ozone, 16 stations had data for nitrogen dioxide, a total of 14 stations had data for both ozone and nitrogen dioxide, and a total of 2 sites had data for formaldehyde. Of those 2 stations, one station, Dallas Hinton, had both 8-hour and 24-hour data while the other station, Fort Worth Northwest, only had 24-hour data. For the San Antonio region, a total of 16 stations had data of which 12 stations had data for ozone, 11 stations had data for nitrogen dioxide, and 7 stations had data for both ozone and nitrogen dioxide. None of the stations had formaldehyde data. For the El Paso region, a total of 8 stations had data of which 7 stations had data for ozone, 4 stations had data for nitrogen dioxide, and 3 stations had data for both ozone and nitrogen dioxide. None of the stations had formaldehyde data. A scan of the Photochemical Assessment Monitoring Stations (PAMS) network was also done but confirmed the lack of stations for San Antonio and El Paso.

Given the sampling constraints of in situ observations, each urban area's ozone production regime was not determined. We focus on four locations only, Deer Park #2 and Clinton sites in Houston, and the Dallas/Fort Worth sites of Hinton and Fort Worth Northwest, where their analysis is considered in Section 5.

4: Ozone Formation Regime Indicators

4.1 Indicator Ratios

The transition point between NO_x-limited or VOC-limited regimes is an important policy-relevant metric (Jin et al., 2020). There are several ozone indicator ratios which are used to define the transition value for VOC to NO_x sensitivity, such as the Sillman indicator ratio of hydrogen peroxide to nitric acid (H_2O_2/HNO_3), L_N/Q which is the ratio of radical loss (L_N) through the reaction with NO_x to the total primary radical production (Q), and the ratio of formaldehyde to nitrogen dioxide (HCHO:NO_2). Here, we place interest on L_N/Q and HCHO:NO_2.

L_N/Q

L_N/Q is an ozone indicator where O_3 sensitivity is evaluated based on the ratio of radical loss (L_N) through the reaction with NO_x to the total primary radical production (Q) (Kleinman, 2005, Kleinman et al., 2001). L_N/Q is the fraction of free radicals removed from the atmosphere by reaction with NO_x, and the remaining fraction removed by combination reactions between free radicals (Kleinman, 2005). The formula gives the power law dependence of ozone production $P(O_3)$ on NO_x concentration, VOC reactivity, and radical production rate. This dependence conveys information on where an air parcel is in the range of the high NO_x regime characterized by polluted conditions to the low NO_x regime characterized by clean atmospheres (Kleinman, 2005). A L_N/Q of 0.5 is considered the explicit transition point between NO_x-limited ($L_N/Q < 0.5$) and VOC-limited ($L_N/Q > 0.5$) regimes. L_N/Q is advantageous when an airshed transitions from high NO_x at a source to lower NO_x downwind, making it a robust indicator in areas of mixed emission sources, like Texas urban areas. However, this indicator is underutilized as it requires constrained quantities of measured chemical species as well as accurate predictions of meteorology and other chemical properties in an airshed (Kleinman et al., 2000; Mazzuca et al., 2016). We apply this indicator ratio to the CAMx simulated conditions in the 2022 ozone season, where we compare it with the Jin et al., 2020 regime definitions in Section 4.

FNR

A commonly used method of regime placement is determined by the formaldehyde (HCHO) to nitrogen dioxide (NO_2) ratio (hereafter FNR or HCHO:NO_2), as indicated by several studies (Souri et al., 2023, Goldberg et al., 2022, Duncan et al., 2010; Jin et al., 2020, 2017; Jin & Holloway, 2015; Martin et al., 2004). The FNR uses HCHO concentration as a proxy for VOC reactivity (Souri et al., 2020). The predictive power of the FNR can be used to tease out drivers of ozone formation through its precursors and illustrate how regimes change spatially and temporally when met with specific chemical and meteorological conditions. Satellite measurements and extensive ground monitoring networks have readily available measurement of HCHO and NO_2. Thus, a number of studies apply this feature and observe how the FNR thresholds vary with different conditions or locations (Choi and Souri, 2015, Jin and Holloway, 2015, Jeon et al., 2018, Jin et al., 2017, Johnson et al., 2024).

When comparing FNR values in these studies, the lack of consistency within the FNR thresholds differentiating the transition in the chemical regimes is apparent, suggesting that absolute values to define O_3 production regimes may depend on the specific datasets used to derive the FNR and/or spatiotemporal conditions under which such datasets are sampled. This inconsistency is likely due to the production of HCHO depending on the available NO_x in an environment, where nonlinearity in HCHO/NO_2 is observed and requires individual calculations of ozone sensitivities for individual environments (Wolfe et al., 2016). As such, Johnson et al. (2024) and Schroeder et al. (2017) question explicitly linking FNRs to chemical regimes due to the inadequacy of our current quantitative understanding of exact FNR threshold values delineating regime transitions. The ambiguity is reflected by the various proposed transition points seen across the literature. Specifically, it was suggested by Martin et al. (2004) that the transition between NO_x-limited and VOC-limited regimes occurs at a HCHO/NO_2 ratio of 1; Duncan et al. (2010) added a "transitional regime" when HCHO/NO_2 ranges from 1 to 2 and stated that NO_x-limited regimes are greater than 2 ($HCHO/NO_2$ >2) and VOC-limited regimes are less than 1 ($HCHO/NO_2$ <1). We see in Souri et al. (2020) that static threshold points misclassify data, and do not consider local features of a region's airshed. More recently, location specific FNR thresholds have been derived by Xiong et al. (2023) for Michigan, Schroeder et al. (2017) for Colorado, and notably for 7 major urban centers in the United States in Jin et al. (2020). Despite concerns, defining a transition point using $HCHO:NO_2$ and regime delineation provides a powerful tool to detect O_3 sensitivity using satellite data which are readily available. Placing airsheds into regimes helps government agencies to quantitatively assess which species are driving ozone production to where emission control strategies could be enacted, and thus carry substantial importance in understanding regional air quality.

5: Indicator Results

L_N/Q

Within the CAMx modeling framework there are ozone indicator ratios which distinguish when and where the ozone production is limited by NO_x or VOCs (CAMx User Guide). Out of the available CAMx options, we utilize the Kleinman L_N/Q ratio described above. **Figure 12** shows the spatial distribution of L_N/Q for the 2022 full ozone season (**Figure 12 a**). Seasonality is present but great variations are not seen as illustrated in **Figure 12 b-d** for the spring (b), summer (c), and fall (d).

Table 1. L_N/Q values for select conditions

	Houston	Dallas	San Antonio	El Paso
All	0.43 ± 0.13	0.39 ± 0.09	0.33 ± 0.13	0.4 ± 0.18
April – May	0.47 ± 0.14	0.43 ± 0.1	0.32 ± 0.1	0.45 ± 0.15
June – August	0.43 ± 0.13	0.34 ± 0.08	0.34 ± 0.17	0.34 ± 0.19
September - October	0.39 ± 0.12	0.43 ± 0.09	0.34 ± 0.13	0.44 ± 0.24
May	0.41 ± 0.14	0.41 ± 0.1	0.29 ± 0.1	0.46 ± 0.16
June	0.34 ± 0.13	0.32 ± 0.09	0.3 ± 0.12	0.32 ± 0.18
August	0.53 ± 0.16	0.37 ± 0.08	0.39 ± 0.2	0.37 ± 0.2
September	0.34 ± 0.13	0.32 ± 0.08	0.32 ± 0.18	0.35 ± 0.23

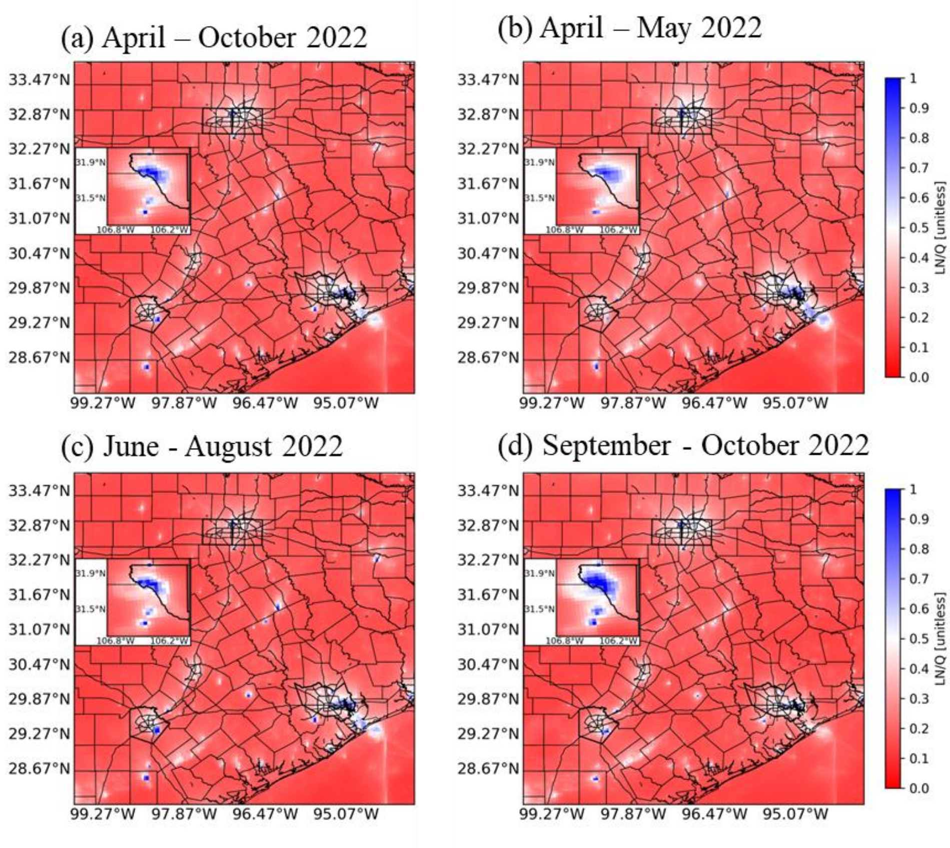

Figure 12. L_N/Q spatial distribution values for all of Texas for (a) the 2022 ozone season (April – October), (b) the spring season (April-May or AM), (c) the summer season (June – August or JJA), and (d) the fall season (September – October or SO) within the 2022 ozone season.

Kleinman (2005) does not set an explicit transitional regime for L_N/Q as this transitional point depends on the contribution of organic nitrates to LN which will vary the transitional point as much as 0.3 depending on the environment. Incorporating this sensitivity factor we define our own transitional regime for L_N/Q. The transitional regime in L_N/Q is set as [0.4-0.6] if the standard deviation of L_N/Q is larger than 0.1. When this condition is met, we categorize an FNR less than 0.4 as NO_x-limited, that greater than 0.6 is VOC-limited. **Table 1** lists the specific L_N/Q values for each county of interest in different seasons and months. **Table 2** includes the individual regime-specific L_N/Q values for other select conditions.

Table 2. L_N/Q values for select conditions

		Houston	Dallas	San Antonio	El Paso
All	NOx-Limited	0.38 ± 0.07	0.38 ± 0.07	0.31 ± 0.08	0.29 ± 0.05
	Transitional				0.48 ± 0.06
	VOC-Limited	0.62 ± 0.09	0.55 ± 0.05	0.71 ± 0.21	0.75 ± 0.13
Weekend	NOx-Limited	0.33 ± 0.08	0.35 ± 0.07	0.29 ± 0.08	0.3 ± 0.08
	Transitional				
	VOC-Limited	0.63 ± 0.1	0.56 ± 0.04	0.71 ± 0.22	0.66 ± 0.12
Weekday	NOx-Limited	0.39 ± 0.07	0.38 ± 0.07	0.32 ± 0.08	0.31 ± 0.06
	Transitional				0.48 ± 0.05
	VOC-Limited	0.61 ± 0.09	0.55 ± 0.05	0.68 ± 0.2	0.77 ± 0.14
Exceedances	NOx-Limited	0.3 ± 0.09	0.32 ± 0.07	0.28 ± 0.08	0.26 ± 0.06
	Transitional				0.5 ± 0.07
	VOC-Limited	0.6 ± 0.07	0.54 ± 0.03	0.74 ± 0.21	0.78 ± 0.14
Temp.Greater 85th%	NOx-Limited	0.31 ± 0.08	0.33 ± 0.08	0.28 ± 0.09	0.33 ± 0.07
	Transitional				
	VOC-Limited	0.6 ± 0.09	0.61 ± 0.06	0.73 ± 0.21	0.66 ± 0.11

L_N/Q is comparable to $(PROOH+PH_2O_2)/PHNO_3$, where then $(PROOH+PH_2O_2)/PHNO_3$ is proportional to $HCHO:NO_2$. We relate L_N/Q and $HCHO:NO_2$ in **Figure 13** for regridded TROPOMI observations and CAMx results in (**a**) Houston, (**b**) Dallas, (**c**) San Antonio, and (**d**) El Paso for the 2022 ozone season. The power law dependence of ozone production $P(O_3)$ on NO_x concentration, VOC reactivity, and radical production rate is observed in **Figure 13**. Relating L_N/Q and FNR shows that maximum FNR values can fall within the L_N/Q-defined NO_x-limited regime, indicating high HCHO and/or small NO_x concentrations. Minimum to median FNR values can fall within either L_N/Q-defined regime, NO_x, or VOC-limited. Minimum values tend to be placed in the L_N/Q-defined VOC-limited regime where high NO_x and/or small HCHO concentrations could occur. The placement of low or high FNR values in the L_N/Q regime definitions is consistent with FNR regime definitions from Jin et al. (2020) and Duncan et al. (2010), where high FNR values are categorized as NO_x-limited and low values are VOC-limited. Yet, as illustrated by **Figure 13**, the FNR regime placement is ambiguous and will depend on local conditions, but there does exist a range which is NO_x-limited specifically near the extremes of the FNR distribution.

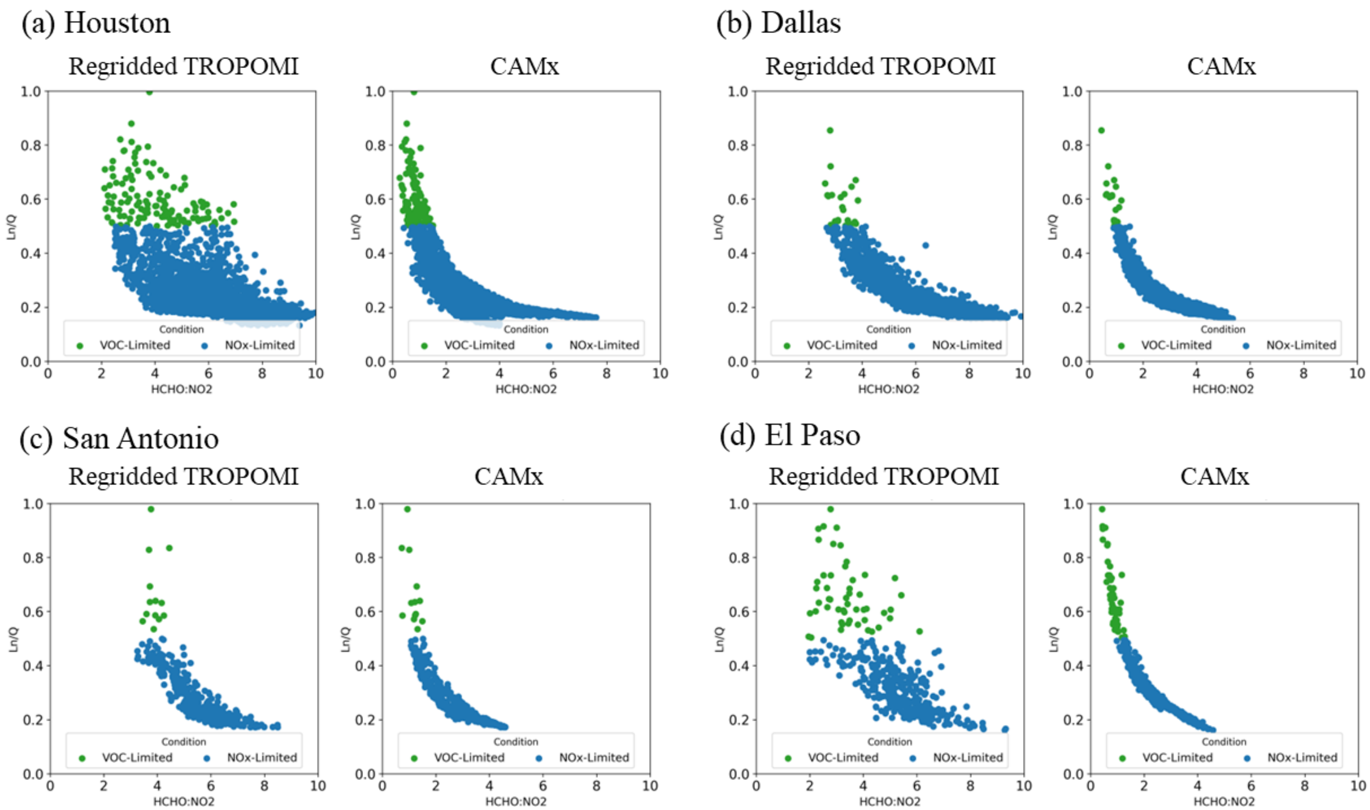

Figure 13. Regridded TROPOMI and CAMx HCHO:NO_2 compared to CAMx simulated L_N/Q for the 2022 ozone season in (a) Houston, (b) Dallas, (c) San Antonio, and (d) El Paso. Blue indicates a NO_x-limited regime when L_N/Q is less that 0.5, and green VOC-limited when L_N/Q is greater than 0.5.

FNR

Focusing on the variations of one year, **Figure 14a-d** displays the FNR from the oversampled TROPOMI observations, regridded TROPOMI observations to match the CAMx resolution, the TROPOMI observations updated with the CAMx calculated AMF, and the CAMx results in molecules/cm^2 for the full ozone season of 2022, where 204 quality observations are employed in the calculations. The FNR varies within each county and with each data product. For each calculated FNR value listed in **Table 3**, values calculated with regridded TROPOMI observations are consistently the highest followed by observations that have been updated with the CAMx AMF or physically oversampled, and the lowest values calculated from CAMx. This behavior is likely due to the differing concentrations of HCHO in TROPOMI observations and CAMx products. The HCHO column within TROPOMI based products see higher concentrations than what is modeled with CAMx (**Figure 9**). The discrepancy of values between the two data products leads to CAMx reporting much lower FNR values than TROPOMI-based products. CAMx values listed in **Table 3** are often 2x lower than what is reported for any TROPOMI-based values.

Following regime definitions from Jin et al., 2020 (further discussed in Section 6), all CAMx-derived FNR values fall in the VOC-limited regimes for each county except for El Paso in June, August, and September which are in the transitional regime. Across the state of Texas more variability is seen in CAMx-derived values where NO_x-limited regimes are present in more suburban and rural regions. TROPOMI-based data products see value and regime variability in each urban area. In the total ozone season (All), Houston, Dallas, and El Paso each fall within the transitional regime, where San Antonio and most of the state are categorized as NO_x-limited consistent with other findings for this area for physically oversampled TROPOMI observation (Goldberg et al., 2022). Houston and Dallas are in the transitional regime while San Antonio and El Paso are in the NO_x-limited regime for TROPOMI with CAMx AMF observations. All counties are in the NO_x-limited regime for regridded TROPOMI observations. Each urban area experiences high and low FNR values compared to other areas in Texas, and consistency is not seen where one location experiences the lowest or highest values.

Seasonality is seen within the FNR values, shown in **Figure 14e-p**. FNR seasonality is largely driven by natural emissions contributing to the HCHO column where the emissions of NMVOCs (non-methane VOCs) from vegetation and the interannual variation of surface temperatures and solar radiation produce this variability (De Smedt et al., 2021). Although not as strong, NO_2 emissions experience seasonality due to stronger photolysis rates heightened by the elevated surface temperatures and solar radiation in the summertime (JJA). We note, however, that HCHO is also affected by these stronger photolysis rates. Anthropogenic emissions of HCHO and NO_2 show less seasonal influences but can be present. Evaporative emissions of anthropogenic volatile organic compounds (AVOCs) are sensitive to ambient temperature and NO_x emissions from electricity-generating units can increase in extreme temperatures (Wu et al., 2024, He et al., 2013). However, Abel et al. (2017) showed that NO_x emissions from electricity-generating units across Texas experience little sensitivity to seasonal factors such as increased temperatures in the summertime (JJA). This leads us to conclude that the seasonality of FNR values in Texas is largely driven by the biogenic emissions affecting HCHO. As such, in **Figure 14**, HCHO column densities increase during summertime, producing higher FNRs (**Figure 14i-l**: JJA) compared to that of spring (**Figure 14e-h**: AM) or fall (**Figure 14m-p**: SO). **Table 3** lists the specific FNR values for each county of interest in different seasons, months, and select conditions.

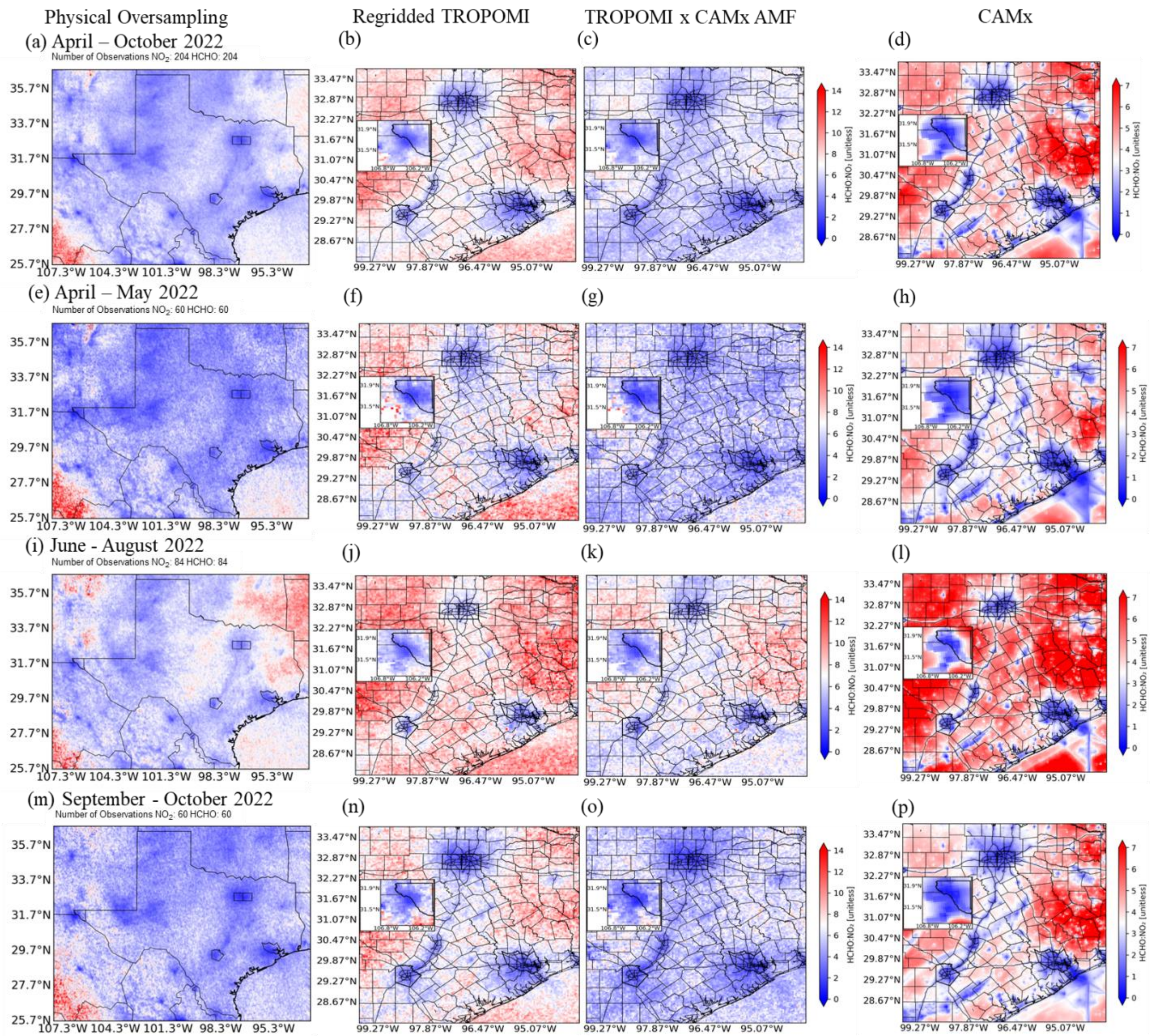

Figure 14. FNR values from oversampled TROPOMI, regridded TROPOMI, TROPOMI x CAMx AMF, and CAMx for all of Texas for (a-d) the 2022 ozone season (April – October). (e-h) shows the spring season (April-May or AM), (i-l) the summer season (June – August or JJA), (m-p) the fall season (September – October or SO) within the 2022 ozone season. The number of observations employed in the calculation is shown directly on the plot.

Table 3. FNR values for select conditions

		Houston	Dallas	San Antonio	El Paso
All	Physical Oversampling	3.14 ± 0.73	3.16 ± 0.47	3.7 ± 0.57	2.99 ± 0.63
	TROPOMI CAMx x AMF	3.25 ± 0.8	3.38 ± 0.64	4.08 ± 0.74	4.03 ± 0.95
	TROPOMI	3.79 ± 0.96	3.89 ± 0.69	5.01 ± 0.86	4.85 ± 1.17
	CAMx	1.52 ± 0.6	1.56 ± 0.53	2.16 ± 0.77	1.95 ± 0.84
April – May	Physical Oversampling	2.76 ± 0.71	2.64 ± 0.48	3.47 ± 0.61	2.13 ± 0.65
	TROPOMI CAMx x AMF	2.93 ± 0.68	3.05 ± 0.57	4.28 ± 0.86	3.21 ± 0.92
	TROPOMI	3.64 ± 0.82	3.73 ± 0.63	5.37 ± 0.93	4.03 ± 1.13
	CAMx	1.25 ± 0.5	1.28 ± 0.44	1.99 ± 0.66	1.39 ± 0.5
June – August	Physical Oversampling	3.86 ± 0.77	4.43 ± 0.54	4.37 ± 0.74	3.75 ± 0.69
	TROPOMI CAMx x AMF	4.31 ± 0.95	4.55 ± 0.8	4.72 ± 1.0	4.74 ± 1.28
	TROPOMI	4.69 ± 1.0	5.28 ± 0.79	5.62 ± 1.16	5.39 ± 1.5
	CAMx	1.58 ± 0.63	1.95 ± 0.69	2.4 ± 0.94	3.05 ± 1.6
September - October	Physical Oversampling	2.67 ± 0.72	2.12 ± 0.43	3.05 ± 0.54	3.03 ± 0.62
	TROPOMI CAMx x AMF	2.97 ± 0.86	2.45 ± 0.7	3.11 ± 0.73	4.24 ± 1.33
	TROPOMI	3.56 ± 1.07	2.81 ± 0.74	3.93 ± 0.79	5.26 ± 1.63
	CAMx	1.71 ± 0.75	1.33 ± 0.45	2.02 ± 0.73	1.57 ± 0.71
May	Physical Oversampling	3.42 ± 0.77	3.6 ± 0.57	4.07 ± 0.62	2.34 ± 0.71
	TROPOMI CAMx x AMF	3.57 ± 1.11	3.95 ± 0.99	4.92 ± 1.18	3.18 ± 1.08
	TROPOMI	4.49 ± 1.37	4.52 ± 0.98	6.1 ± 1.26	4.13 ± 1.38
	CAMx	1.49 ± 0.64	1.34 ± 0.46	2.4 ± 0.88	1.48 ± 0.55
June	Physical Oversampling	4.11 ± 0.72	4.41 ± 0.50	4.4 ± 0.56	3.6 ± 0.66
	TROPOMI CAMx x AMF	4.52 ± 1.14	4.6 ± 1.07	4.65 ± 1.17	4.4 ± 1.37
	TROPOMI	4.92 ± 1.19	5.35 ± 1.06	5.62 ± 1.3	5.33 ± 1.71
	CAMx	2.24 ± 1.07	1.98 ± 0.64	2.66 ± 1.05	2.83 ± 1.54
August	Physical Oversampling	3.3 ± 1.03	4.15 ± 1.03	4.21 ± 1.06	4.04 ± 0.69
	TROPOMI CAMx x AMF	4.36 ± 1.23	4.33 ± 1.15	4.41 ± 1.24	5.84 ± 2.02
	TROPOMI	5.08 ± 1.39	5.33 ± 1.3	5.53 ± 1.49	6.53 ± 2.11
	CAMx	1.2 ± 0.5	1.81 ± 0.63	2.0 ± 0.76	2.99 ± 1.6
September	Physical Oversampling	3.38 ± 0.71	2.75 ± 0.73	3.57 ± 0.88	3.85 ± 0.70
	TROPOMI CAMx x AMF	3.64 ± 1.08	2.95 ± 0.9	3.7 ± 1.06	5.82 ± 2.29
	TROPOMI	4.39 ± 1.31	3.63 ± 1.03	4.18 ± 1.03	6.98 ± 2.48
	CAMx	2.08 ± 0.98	1.8 ± 0.65	2.45 ± 0.93	2.72 ± 1.44

The results further reveal that TROPOMI and CAMx observations are still able to resolve the seasonality in one-month averaged FNR values, using 30 or 31 corresponding observations as shown in **Figure 15.** The months of May, June, and September experienced the highest number of monthly ozone exceedances throughout the 5-year period (https://www.tceq.texas.gov/cgi-bin/compliance/monops/8hr_exceed.pl.) and were selected due to this reason. With a visual inspection, June (**Figure 15e-h**) sees an increase in the HCHO column across central and east Texas compared to that of May (**Figure 15a-d**) and September (**Figure 15m-p**). Compared to their seasonal average, shown in **Figure 14**, May and September experience higher FNRs, whereas June doesn't experience an overall increase or decrease with its seasonal average. Increasing the FNR from seasonal averages suggests that an increase in the HCHO column during these months, increased photolysis rates of NO_2 due to higher temperatures that seasonal counterparts, or a lower NO_2 column could drive high levels of ozone contributing to concentrations exceeding the national standard.

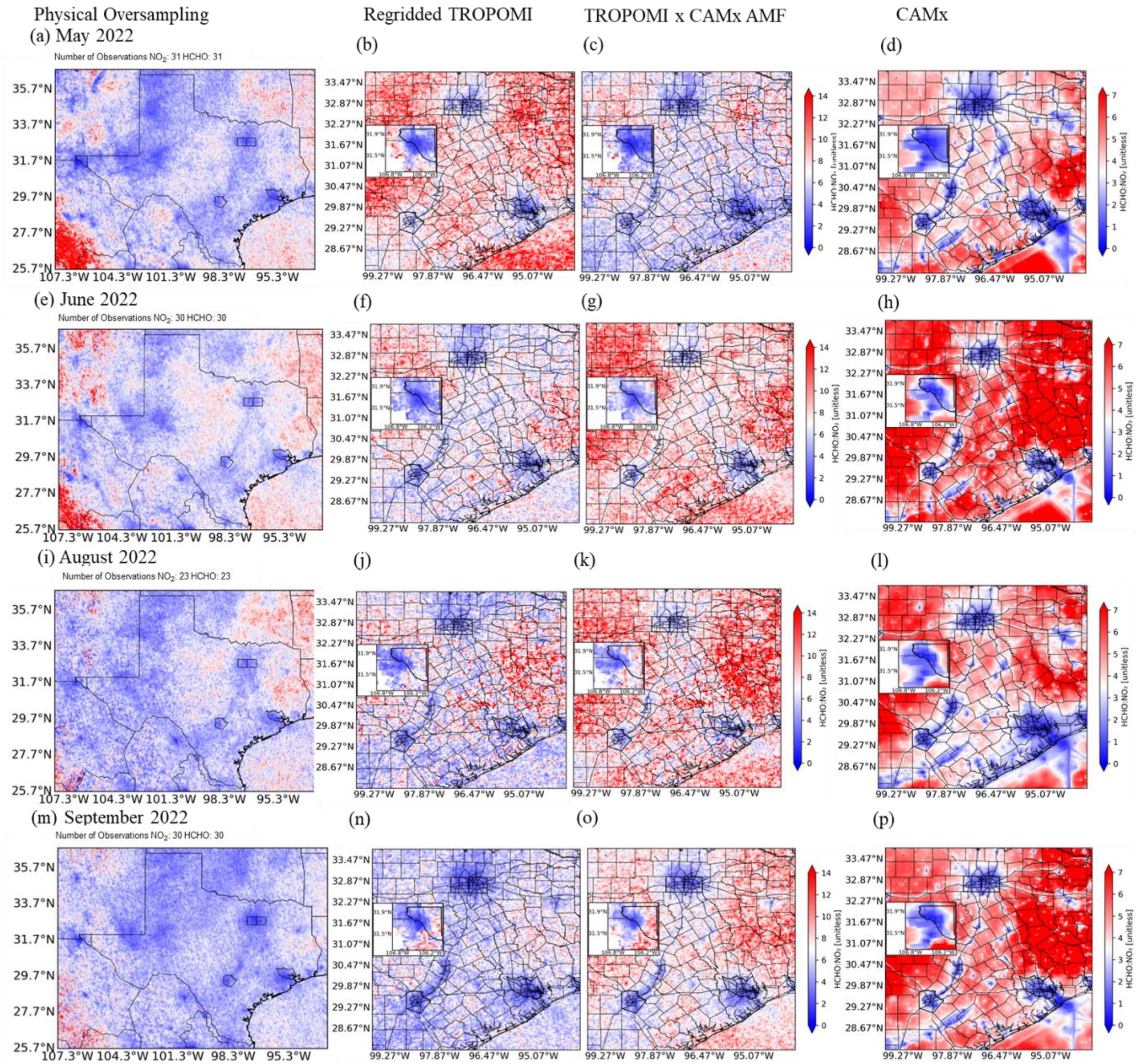

Figure 15. FNR values from oversampled TROPOMI, regridded TROPOMI, TROPOMI x CAMx AMF, and CAMx for all of Texas for the months of (a-d) May (e-h) June, (i-l) August, and (m-p) September 2022. The number of observations employed in the calculation is shown directly on the plot.

We excluded in totality days where there was not 85% pixel coverage in a defined area such as the whole of Texas or within each county of interest being Harris County for Houston, Bexar County for San Antonio, El Paso County for El Paso, and Tarrant and Dallas County for Dallas. Excluding the cloud-covering days had little effect on the results as when clouds obstruct the view of the satellite no data is recorded and thus are not included in calculations. Excluding the cloud-covering days does not contribute to the average FNR for the period. Thus, the observed residual 25% of the NO_2 pixels captured by TROPOMI observations could serve to increase or decrease the average given the value of the excluded pixels. Additionally, the Texas region is frequently covered by two overpasses or swaths of TROPOMI. The swaths covering the region are merged and/or averaged when performing oversampling following Sun et al. (2018), regidding to match the CAMx domains, and updating the TROPOMI AMF with a newly derived AMF based on CAMx products. This leads to the region of Texas seeing fewer pixels removed due to clouds or our user-defined quality checks, as shown in **Table 4**.

Table 4. The number of cloud-free days included in FNR calculations and that excluded by month in 2022 for the Texas domain shown in the above **Figure 14**.

	Cloud-Free NO_2	**Cloud-Free HCHO**	**Cloud-Covering NO_2**	**Cloud-Covering HCHO**	**Did not pass quality checks or missing data NO_2**	**Did not pass quality checks or missing data HCHO**
Total	122	115	1	1	1	8
April	29	29	1	1	0	0
May	31	31	0	0	0	0
June	30	30	0	0	0	0
July	31	31	0	0	0	0
August	31	23	0	0	0	8
September	30	30	0	0	0	0
October	30	31	0	0	1	0

Oversampled satellite observations were then compared to surface monitors within the ground network run by the TCEQ. Due to data constraints, only four sites were analyzed: (1) Houston: Deer Park #2, (2) Houston: Clinton, (3) Dallas: Hinton, and (4) Dallas: Fort Worth Northwest. Houston: Deer Park #2 is located in the southeast corner of Houston and is near the Houston Ship Channel and La Porte Airport. Houston: Clinton is located in east Houston near the Houston Ship Channel and the major roadway Intersate-610. Dallas: Hinton is near the University of Texas Southwestern Medical Center and Highway 77/35, one of the major highways that runs through the center of Dallas. Dallas: Fort Worth Northwest is just south of the Fort Worth Meacham International Airport near the railroad network and the Dallas Area Rapid Transit lines. The varying site locations influence the FNR values due to site-specific emission make-ups.

The variations in the surface FNR value compared to oversampled TROPOMI observations for the 2022 total ozone season are shown in **Figure 16**. In **Figure 16**, there is little numerical similarity between the surface and satellite observation, but Houston Deer Park #2 (**Figure 16a**) and Dallas Hinton (**Figure 16c**) show periods where the trend in FNR values do align in the summer months of June and July. Considering the condition of ozone exceedance days, the FNR values vary between surface and satellite observations, but regime placement, when following Jin et al. (2020) or Blanchard (2020), is often similar across all four sites. When analyzing **Figure 16a**, we see the regime placement is similar between surface and oversampled TROPOMI observations for three out of four exceedance days shown with available observations. The corresponding regimes for these exceedance days are VOC-limited. Similar behavior is seen within each site shown in **Figure 16**. The regime placement throughout the period for oversampled TROPOMI is variable and reflects the site's location as well as only choosing a single TROPOMI grid to compare with surface monitors. Surface regime placement is variable too, but a trend is seen with FNR values reaching maximums in summer months (JJA) and pushing these sites to be more frequently considered transitional or NO_x-limited. Higher FNRs observed in summer months could be due to higher HCHO concentrations observed (see **Appendix: Figure 1**).

FNR values calculated from surface observations mainly stayed within either the VOC-limited or the transitional regime for all four sites. The Houston sites tend to stay near the VOC-limited regime while Dallas sites tend to stay within the transitional regime. Further analysis with surface observations are not seen in the rest of this report due to data limitations.

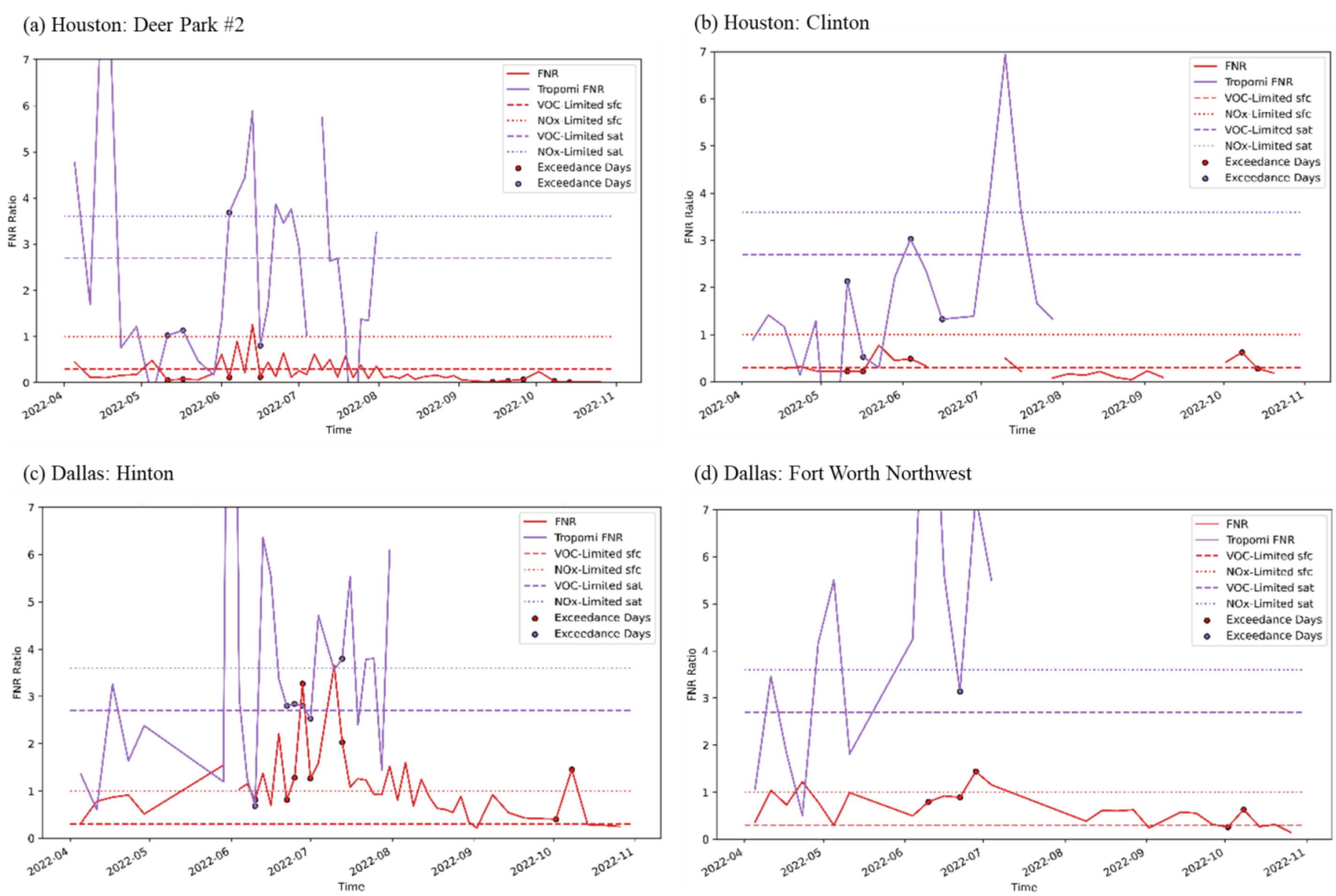

Figure 16. Time series of FNR for surface (red) and oversampled TROPOMI (purple) observations at 4 surface monitor locations in (a) Houston: Deer Park #2, (b) Houston: Clinton, (c) Dallas: Hinton, and (d) Dallas: Fort Worth Northwest. Solid red lines are surface and solid purple lines are satellite FNR values. Ozone exceedance days are denoted by circles and are color coded to match the color of the lines for surface (red) and satellite (purple) observations. Ozone production regimes are denoted, dotted line indicates NO_x-limited regime line and dashed line indicates VOC-limited regime line. Surface regime values are from Blanchard (2020) and satellite regime lines are from Jin et al., (2020).

Figure 17 a-e shows the density distribution of the oversampled TROPOMI monthly mean FNRs throughout the 5-year period within each county, while **Figure 17 f-j** shows the density distribution for 2022 CAMx results for All, Exceedances, Weekends, and Weekdays. Overall, there is a generally normal distribution for each condition. In oversampled TROPOMI, All and Weekdays see a breakdown of this normal distribution experiencing a leftward skew, which could be indicative of the higher NO_x emissions occurring on weekdays. weekdays, throughout all counties, experience a lower FNR than all conditions. The density of weekends sees a higher FNR than weekdays but not for all conditions in each county. This weekday-weekend FNR relation could be attributed to the understanding of increased NO_x emissions from the anthropogenic sector on weekdays compared to that on weekends (Goldberg et al., 2021). The proportion of exceedance days encompassing all counties exhibits a higher FNR compared to that of other conditions (**Figure 17a**). However, individual counties see this relation break, specifically in El Paso (**Figure 17d**) and Dallas (**Figure 17c**), pointing to the complexity of O_3 formation on exceedance days. Focusing on CAMx simulated FNRs, **Figure 17 f-j** seems a similar normal distribution for all counties and conditions with slightly increased density and FNR values observed than oversampled TROPOMI observations. Each location sees a similar density pattern with exceedances seeing the highest density distribution followed by weekend, all, and weekday with the lowest. In the CAMx model, the portion of exceedance days sees a higher FNR consistent with oversampled TROPOMI, and a limited range of FNR values in this condition when compared to other conditions. The normal distribution slightly breaks for each urban area, but the location of the break occurs both before and after the peak density point, illustrating the variability of FNR values.

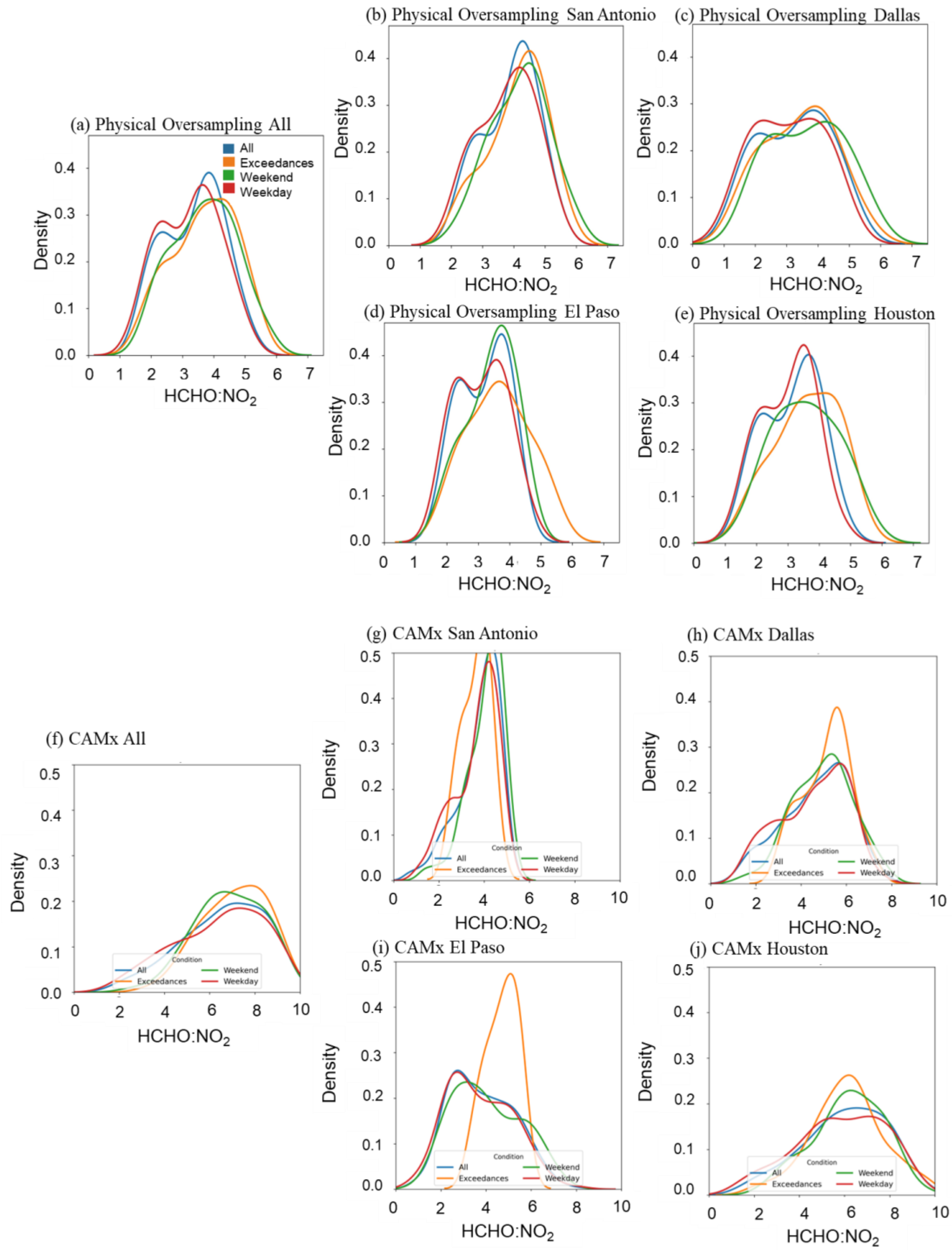

Figure 17. Density distribution of average monthly TROPOMI derived HCHO: NO_2 ratios conditions between the years of 2019-2022. The four counties of interest were combined to produce yearly averages using Physical Oversampled TROPOMI observations for (a) All and then each county of interest being Bexar County for (b) San Antonio, Tarrant, and Dallas County for (c) Dallas, El Paso County for (d) El Paso, and Harris County for (e) Houston was separated. The density distribution of CAMx data products are shown in (f) All and then each county of interest being Bexar County for (g) San Antonio, Tarrant, and Dallas County for (h) Dallas, El Paso County for (i) El Paso, and Harris County for (j) Houston. Note the differing x- and y- axis for a-e and f-j.

6: Jin et al. (2020) Regime Definitions Overview and Application

The Jin et al. (2020) method is a powerful means for determining O_3 sensitivity as it does not use a photochemical box model, chemical transport modeling simulations, or extensive field campaigns. The method allows for O_3 precursor species which are remotely sensed at high frequency and are readily available to be used in describing the local tendency of O_3 production in a region. It only uses the HCHO:NO_2 indicator and does not require extensive chemical analyses of other ozone-influencing species like other ozone indicator ratios may require. Here, we first apply the Jin et al., 2020 regime definitions to Texas urban areas for all intercomparison products. We will analyze the methodology and share findings, and lastly we will apply the methodology to oversampled TROPOMI NO_2 and HCHO observations and a simulated atmospheric environment from the CAMx photochemical simulations.

Jin et al. (2020) found the high-O_3 probability peaks at HCHO/NO_2 at 3.1 for Houston, and its FNR transitional regime is defined to be [2.7, 3.6] after 2009. Thus, in this study, we adapt these defined regime boundaries and categorize an FNR greater than 3.6 as NO_x-limited, that less than 2.7 is VOC-limited, and [2.7, 3.6] as transitional. **Figure 18** shows the spatial distribution of the FNR and regime classification for the 4 urban areas based on Jin et al. (2020) thresholds. The large differences in the FNR between the four products result in a very different regime delineation in each urban area when applied with the same thresholds from Jin et al. (2020).

The regime pattern is similar in each urban area but with each data product, there are spatial changes in regime placement. Similarly, we see that the NO_x-limited regime dominates the rural to suburban areas, and as one approaches the city center or large emission points we enter a transitional or VOC-limited regime. The VOC-limited regime carries the smallest spatial area and is found in areas that are dominated by NO_x emissions, which are observed in the central areas of the counties and are co-located with their major urban areas or large emission points. CAMx results (**Figure 18 m-p**) see the largest VOC-limited regimes suggesting that the model is heavily emission-driven, and VOC-limited regime placement is a response to where the highest NO_x emissions are found, such as city centers and roadways. TROPOMI-based data products do not see such a dominant VOC-limited regime which could be due to the satellite's inability to resolve fine-scale features given its spatial footprint (i.e. 3.5×5.6 km^2 at nadir) or the influence of emission inventories used within a model framework in which satellite's do not have. The transitional and VOC-limited regime is limited in Regridded TROPOMI (**Figure 18 e- h**) indicating that the NO_2 column is lower than that observed in CAMx or Physical Oversampling products. When the CAMx AMF is introduced or the TROPOMI product follows a physical oversampling process, the transitional and VOC-limited regimes see an increase in their spatial breath, suggesting that alteration of the raw data product is needed to capture increases and additional spatial variability in NO_2 across these urban areas.

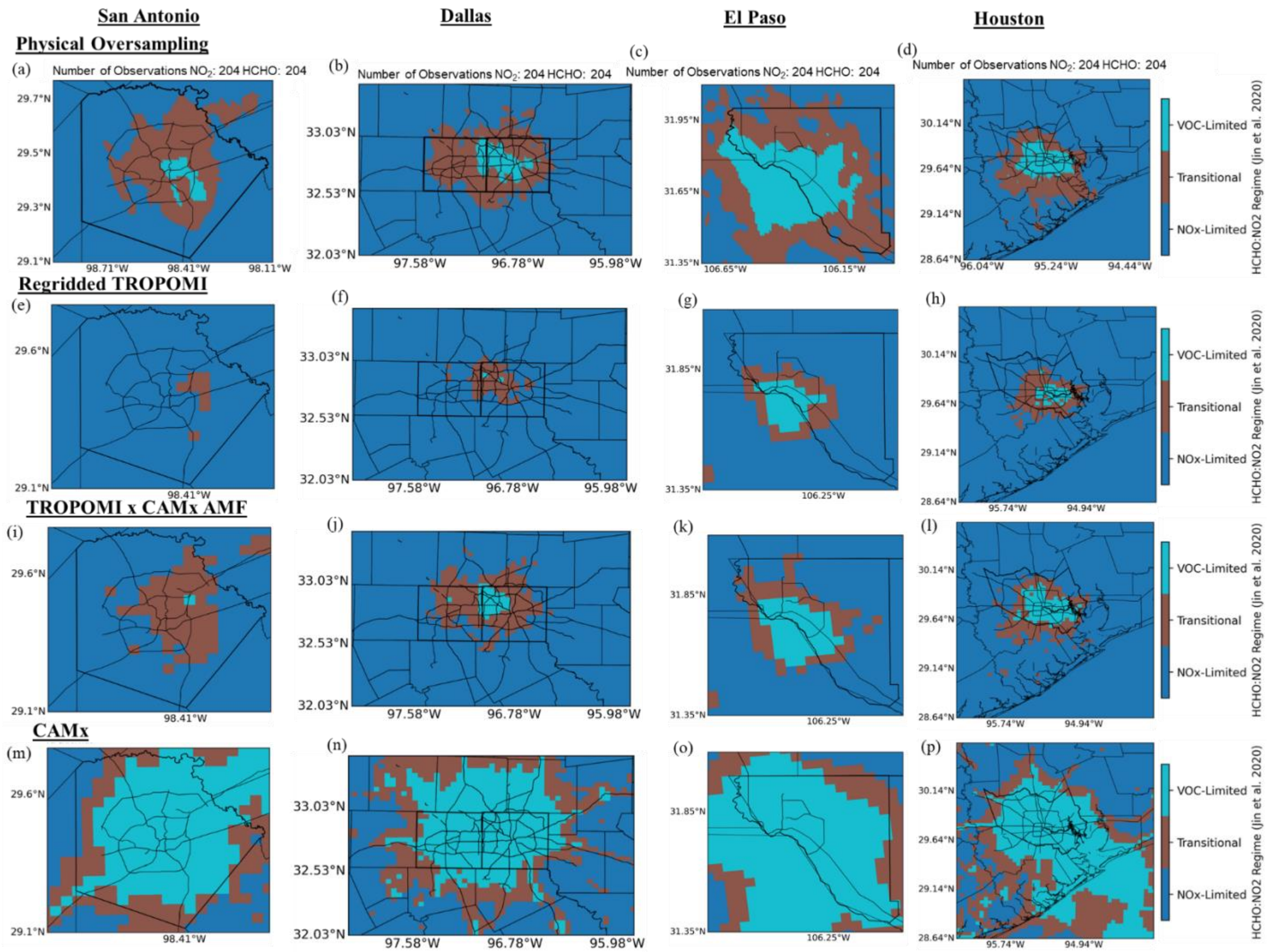

Figure 18. Physical Oversampled TROPOMI (a-d), TROPOMI- (e-h), TROPOMI x CAMx AMF, (i-l) and CAMx (m-p) derived FNR values for counties of interest for select conditions being the 2022 ozone season and placed within regimes defined by Jin et al., (2020).

Table 5. FNR regimes values for the four counties of interest for select conditions defined by Jin et al., 2020 regime for Houston, TX applied to all counties. Blank values indicate no regime was found.

			Houston	Dallas	San Antonio	El Paso
All	Physical Oversampling	NOx-Limited	4.08 ± 0.35	3.88 ± 0.22	4.09 ± 0.34	3.89 ± 0.29
		Transitional	3.13 ± 0.27	3.16 ± 0.24	3.19 ± 0.27	3.14 ± 0.25
		VOC-Limited	2.41 ± 0.21	2.51 ± 0.13	2.62 ± 0.05	2.25 ± 0.32
	TROPOMI CAMxAMF	NOx-Limited	4.14 ± 0.4	4.11 ± 0.35	4.44 ± 0.58	4.56 ± 0.58
		Transitional	3.11 ± 0.25	3.2 ± 0.25	3.26 ± 0.22	3.24 ± 0.26
		VOC-Limited	2.4 ± 0.21	2.52 ± 0.13	2.68 ± 0.2	2.3 ± 0.23
	TROPOMI	NOx-Limited	4.55 ± 0.61	4.29 ± 0.51	5.07 ± 0.81	5.21 ± 0.9
		Transitional	3.08 ± 0.24	3.2 ± 0.25	3.42 ± 0.14	3.14 ± 0.28
		VOC-Limited	2.49 ± 0.17	2.64 ± 0.04		2.48 ± 0.11
	CAMx	NOx-Limited	3.61 ± 0.1	3.62 ± 0.22	3.91 ± 0.21	3.76 ± 0.11
		Transitional	3.03 ± 0.25	3.09 ± 0.27	3.09 ± 0.26	3.05 ± 0.26
		VOC-Limited	1.42 ± 0.47	1.48 ± 0.39	1.79 ± 0.49	1.65 ± 0.64
Weekend	Physical Oversampling	NOx-Limited	3.15 ± 0.26	3.25 ± 0.25	3.16 ± 0.23	3.12 ± 0.25
		Transitional	2.50 ± 0.09	2.58 ± 0.14	2.55 ± 0.09	2.36 ± 0.26
		VOC-Limited	1.42 ± 0.47	1.48 ± 0.39	1.79 ± 0.49	1.65 ± 0.64
	TROPOMI CAMxAMF	NOx-Limited	4.6 ± 0.73	4.62 ± 0.64	4.89 ± 0.84	4.66 ± 0.72
		Transitional	3.21 ± 0.27	3.32 ± 0.2	3.27 ± 0.27	3.17 ± 0.23
		VOC-Limited	2.5 ± 0.13	2.66 ± 0.11	2.57 ± 0.21	2.34 ± 0.31
	TROPOMI	NOx-Limited	4.83 ± 0.86	5.15 ± 0.77	5.83 ± 1.12	5.32 ± 1.04
		Transitional	3.2 ± 0.26	3.45 ± 0.12	3.4 ± 0.17	3.18 ± 0.23
		VOC-Limited	2.6 ± 0.07	3.85 ± 0.2		2.31 ± 0.15
	CAMx	NOx-Limited	3.96 ± 0.28		4.0 ± 0.3	3.76 ± 0.1
		Transitional	3.1 ± 0.22	3.02 ± 0.28	3.17 ± 0.25	3.16 ± 0.26
		VOC-Limited	1.58 ± 0.47	1.69 ± 0.4	1.84 ± 0.44	1.7 ± 0.62
Weekday	Physical Oversampling	NOx-Limited	3.15 ± 0.26	3.09 ± 0.23	3.19 ± 0.25	3.13 ± 0.25
		Transitional	2.32 ± 0.24	2.42± 0.18	2.56 ± 0.08	2.19 ± 0.35
		VOC-Limited	1.58 ± 0.47	1.69 ± 0.4	1.84 ± 0.44	1.7 ± 0.62
	TROPOMI CAMxAMF	NOx-Limited	4.07 ± 0.37	3.99 ± 0.35	4.35 ± 0.54	4.59 ± 0.66
		Transitional	3.12 ± 0.25	3.14 ± 0.24	3.19 ± 0.23	3.18 ± 0.24
		VOC-Limited	2.23 ± 0.28	2.39 ± 0.2	2.5 ± 0.12	2.28 ± 0.28
	TROPOMI	NOx-Limited	4.36 ± 0.63	4.22 ± 0.49	4.8 ± 0.75	5.19 ± 0.93
		Transitional	3.13 ± 0.27	3.17 ± 0.26	3.34 ± 0.24	3.2 ± 0.27
		VOC-Limited	2.42 ± 0.2	2.53 ± 0.08		2.5 ± 0.16
	CAMx	NOx-Limited			3.97 ± 0.19	
		Transitional	3.01 ± 0.18	3.13 ± 0.27	3.08 ± 0.24	3.12 ± 0.23
		VOC-Limited	1.35 ± 0.47	1.43 ± 0.39	1.76 ± 0.5	1.62 ± 0.64
Exceedances	Physical Oversampling	NOx-Limited	4.38 ± 0.58	4.01 ± 0.33	4.5 ± 0.93	4.27 ± 0.54
		Transitional	3.11 ± 0.27	3.19 ± 0.26	3.16 ± 0.26	3.18 ± 0.24
		VOC-Limited	2.38 ± 0.23	2.51 ± 0.14	2.57 ± 0.11	2.34 ± 0.25
	TROPOMI CAMxAMF	NOx-Limited	4.57 ± 0.79	4.36 ± 0.56	5.57 ± 1.87	5.46 ± 1.27
		Transitional	3.09 ± 0.25	3.15 ± 0.27	3.14 ± 0.23	3.15 ± 0.3
		VOC-Limited	2.39 ± 0.21	2.5 ± 0.15	2.32 ± 0.31	2.28 ± 0.35
	TROPOMI	NOx-Limited	4.92 ± 0.97	4.57 ± 0.69	5.28 ± 1.73	5.45 ± 1.29
		Transitional	3.18 ± 0.25	3.17 ± 0.23	3.18 ± 0.26	3.22 ± 0.25
		VOC-Limited	2.51 ± 0.15	2.66 ± 0.01	2.39 ± 0.14	2.26 ± 0.43
	CAMx	NOx-Limited	4.43 ± 0.76	4.17 ± 0.29	4.39 ± 0.54	4.57 ± 0.68
		Transitional	3.14 ± 0.27	2.96 ± 0.24	3.16 ± 0.27	3.12 ± 0.22
		VOC-Limited	1.56 ± 0.48	1.75 ± 0.41	1.79 ± 0.47	1.74 ± 0.64
Temp.Greater 85th%	Physical Oversampling	NOx-Limited	4.55 ± 0.74	4.54 ± 0.57	4.88 ± 0.81	4.44 ± 0.77
		Transitional	3.12 ± 0.26	3.34 ± 0.20	3.22 ± 0.27	3.21 ± 0.25
		VOC-Limited	2.37 ± 0.27	2.67 ± 0.01	2.35 ± 0.22	2.30 ± 0.29
	TROPOMI CAMxAMF	NOx-Limited	4.75 ± 0.86	4.81 ± 0.91	5.22 ± 1.06	4.82 ± 0.97
		Transitional	3.14 ± 0.26	3.2 ± 0.26	3.29 ± 0.17	3.15 ± 0.19
		VOC-Limited	2.4 ± 0.25	2.57 ± 0.1	2.48 ± 0.13	2.26 ± 0.34
	TROPOMI	NOx-Limited	4.96 ± 1.07	5.09 ± 0.91	5.96 ± 1.32	5.26 ± 1.18
		Transitional	3.14 ± 0.25	3.34 ± 0.2	3.12 ± 0.23	3.2 ± 0.24
		VOC-Limited	2.41 ± 0.23			2.33 ± 0.25
	CAMx	NOx-Limited	4.28 ± 0.5	4.44 ± 0.49	4.31 ± 0.46	
		Transitional	3.11 ± 0.22	3.07 ± 0.27	3.1 ± 0.27	3.0 ± 0.2
		VOC-Limited	1.72 ± 0.46	1.69 ± 0.42	1.82 ± 0.4	1.71 ± 0.63

Jin et al. (2020) derived the FNR thresholds using a conceptual framework proposed by Psuede et al. (2012) which used the O_3 exceedance probability to categorize the nonlinear dependence of O_3 production on NO_2 and HCHO. This framework does not consider meteorology so measured O_3 is sensitive to only its local chemical production. Additionally, it assumes that local changes in chemical or depositional loss of O_3 are insignificant on average. Jin et al., 2020 calculates high-O_3 probability when surface O_3 exceeds 70 ppbv at OMI overpass in relation to the relative OMI NO_2 and HCHO. Specifically, high-O_3 probability is calculated by matching hourly EPA Air Quality System (AQS) O_3 observations at the time of OMI overpass (13:30 LT) with daily OMI HCHO/NO_2. Paired observations are placed into 100 bins based on OMI HCHO/NO_2, and the probability of high-O_3 (>70 ppbv) is calculated for each OMI HCHO/NO_2 bin (number of observations which exceeds 70 ppbv within a bin/total number of observations within a bin). Adapted from Jin et al., 2020 Supplementary Information (SI), **Figure 19** shows this application for the 7 cities studied, where the x-axis is the OMI HCHO/NO_2 bin and the y-axis is the high-O_3 probability. The solid black line is the moving average, the 2nd-degree polynomial model is in blue, and the 3rd-degree polynomial model is in orange. The 3rd-degree polynomial model is selected to derive the maximum high-O_3 probability (the peak of the curves) as reported, it best fits the data with the smallest uncertainty estimated by statistical bootstrapping (Jin et al., 2020). The transition point in this model is assumed to be the peak of the curve as marks the transition from VOC-limited to NO_x-limited regimes, and so the transitional regime is defined to be the range of HCHO/NO_2 spanning the top 10% of the high-O_3 probability distribution.

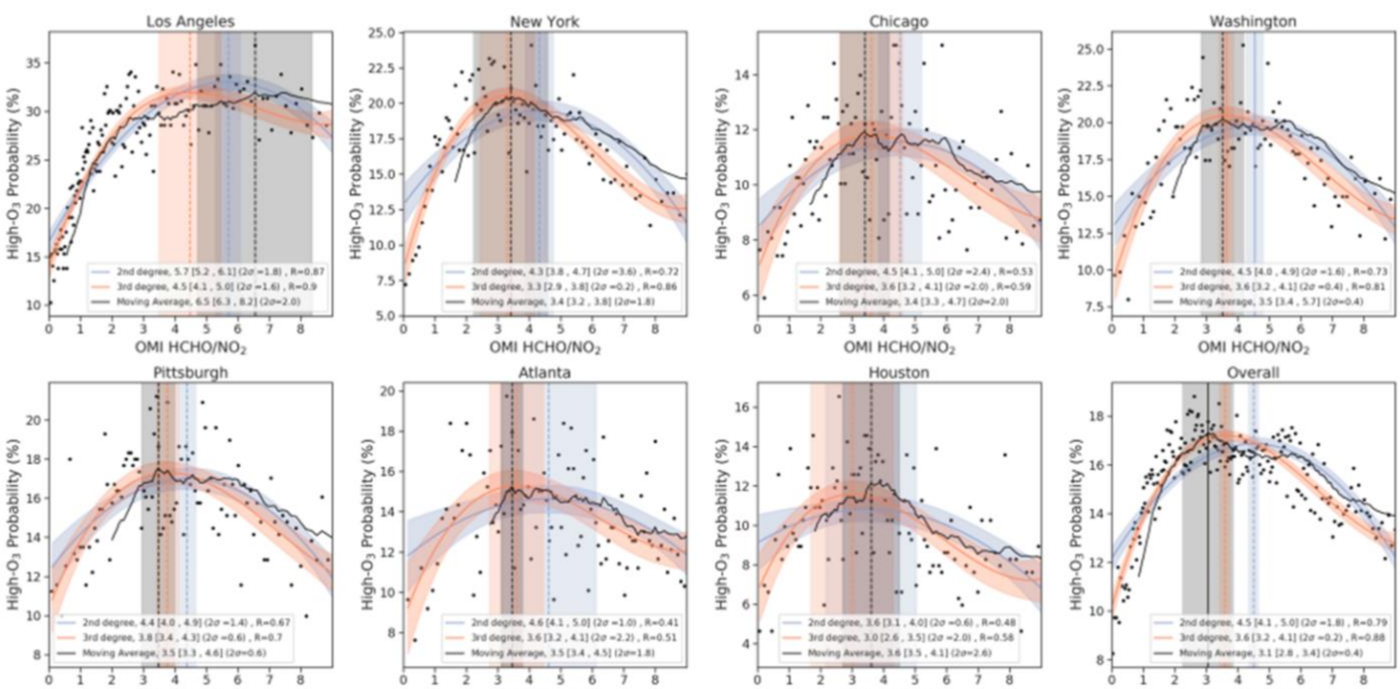

Figure 19. Adapted from Jin et al., 2020: Probability of O_3 exceeding 70 ppbv as a function of OMI HCHO/NO_2 for all select seven cities individually using three models: (1) moving average (black), (2) 2nd-degree polynomial model (blue), and (3) 3rd-degree polynomial model (orange). R is the Pearson correlation coefficient between predictor and predicted values.

When analyzing **Figure 19**, one cannot help but notice the poor agreement between the 3rd-order polynomial and the data for Houston. Poor agreement is likely observed due to the influence of factors such as varying meteorology, chemical and depositional loss of O_3, noise in the satellite retrievals, and the spatial mismatch between the surface O_3 point measurements and the area satellite observations (Jin et al., 2020). We caution the use of regime delineations from Jin et al., 2020 due to the lack of agreement and high standard deviation. More appropriate would be the use of the 'Overall' results where multiple cities are merged as one dataset, where the 3rd order polynomial describes the observations with a high degree of agreement (R=0.88), but the "Overall" results do not consider local chemical variables or region-specific influences and might have achieved a better fit simply due to more data points averaged over each bin.

Applying the Jin et al. (2020) delineations to current conditions can lead to incorrect conclusions and misappropriation of airsheds, requiring the use of more recent observations to build regime definitions. We apply the Jin et al., 2020 methodology for regime delineation to 2018-2023 oversampled TROPOMI NO_2 and HCHO observations (**Figure 20**), 2022 surface-level CAMx simulated NO_2 and HCHO (**Figure 21**) with AQS monitor concentrations of O_3, and 2022 surface-level CAMx simulated NO_2 and HCHO (**Figure 22**) with simulated O_3. We find that high-O_3 probability peaks at oversampled TROPOMI HCHO/NO_2 at values higher than described in Jin et al., 2020. This could be due to features such as low-biased TROPOMI NO_2 (Judd et al., 2020), high-biased TROPOMI HCHO in low and medium columns (De Smedt et al., 2018), or that NO_2 is steadily decreasing across the United States (Jin et al., 2020, Geddes et al., 2016) and thus in Texas urban areas leading to higher FNRs. Higher FNR thresholds imply that areas will be more widely categorized as NO_x-limited and changes in NO_x concentrations will be important to control for limiting high-O_3 production. The oversampled TROPOMI HCHO/NO_2 describing the regime transition varies slightly among urban areas, which is highest in San Antonio (4.5 [4.2-4.9]), followed by Houston (4.4 [4.0-4.9]) and Dallas (3.2 [2.9-3.6]), where El Paso (2.8 [2.4-3.3]) has the lowest transition point.

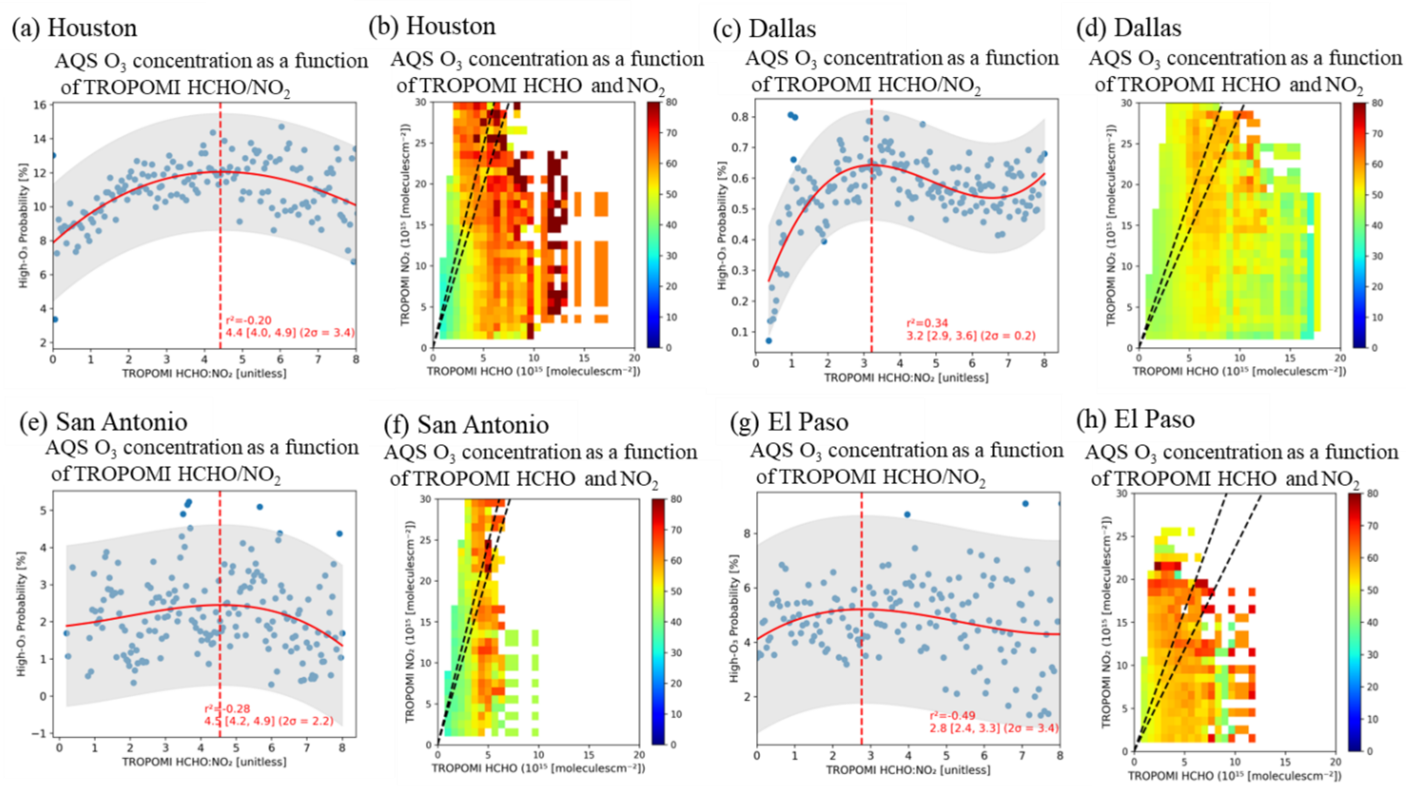

Figure 20. Oversampled TROPOMI-derived regimes following Jin et al., 2020 methodology. Regimes in a, c, e, g are constructed by matching AQS O_3 concentration to its TROPOMI HCHO/NO_2 concentration. The solid lines are fitted third-order polynomial curves, and the shading indicates 95% confidence intervals. The vertical dashed lines indicate the maximum of the fitted curve (labeled in the legend). The uncertainty is two standard deviations (2σ or 95% confidence interval) and the correlation coefficient is listed in the legend. AQS O3 concentration as a function of TROPOMI HCHO and NO_2 in b, d, f, h. The

black dashed lines delineate TROPOMI HCHO/NO$_2$ at the derived transitional regime listed in the legend.

We relax the method and use O$_3$ concentration rather than O$_3$ probability due to the short temporal time frame (i.e., 1 year vs 10 years as in Jin et al., 2020) for transition values calculated with CAMx products. Two approaches were taken to try to achieve a high degree of agreement between HCHO/NO$_2$ and O$_3$ and consider surface conditions when calculating transition values for the individual Texas urban areas, (1) CAMx HCHO/NO$_2$ with AQS observations (CAMx-AQS, **Figure 21)** and (2) CAMx HCHO/NO$_2$ with CAMx O$_3$ (CAMx-CAMx, **Figure 22**). Like TROPOMI-derived transition points, CAMx-AQS transition points result in higher values than the Jin et al., 2020 method. In comparing TROPOMI and CAMx-AQS results, we find good agreement with transition points for Houston (4.4 [4.1-4.8) and El Paso (2.1 [2.0-2.3]), but San Antonio (1.5 [1.4-1.7]) and Dallas (2.9 [2.6-3.4]) see less consistency. All CAMx-derived transition points are found to be slightly lower than that of TROPOMI. Lower CAMx-FNR transition points could be due to low HCHO concentrations when compared to TROPOMI and points to the model's difficulty in simulating complex VOC chemistry. An increase in uncertainty is seen in results with CAMx-AQS due to the comparison of simulated products with ground observations and due to the use of fewer observations.

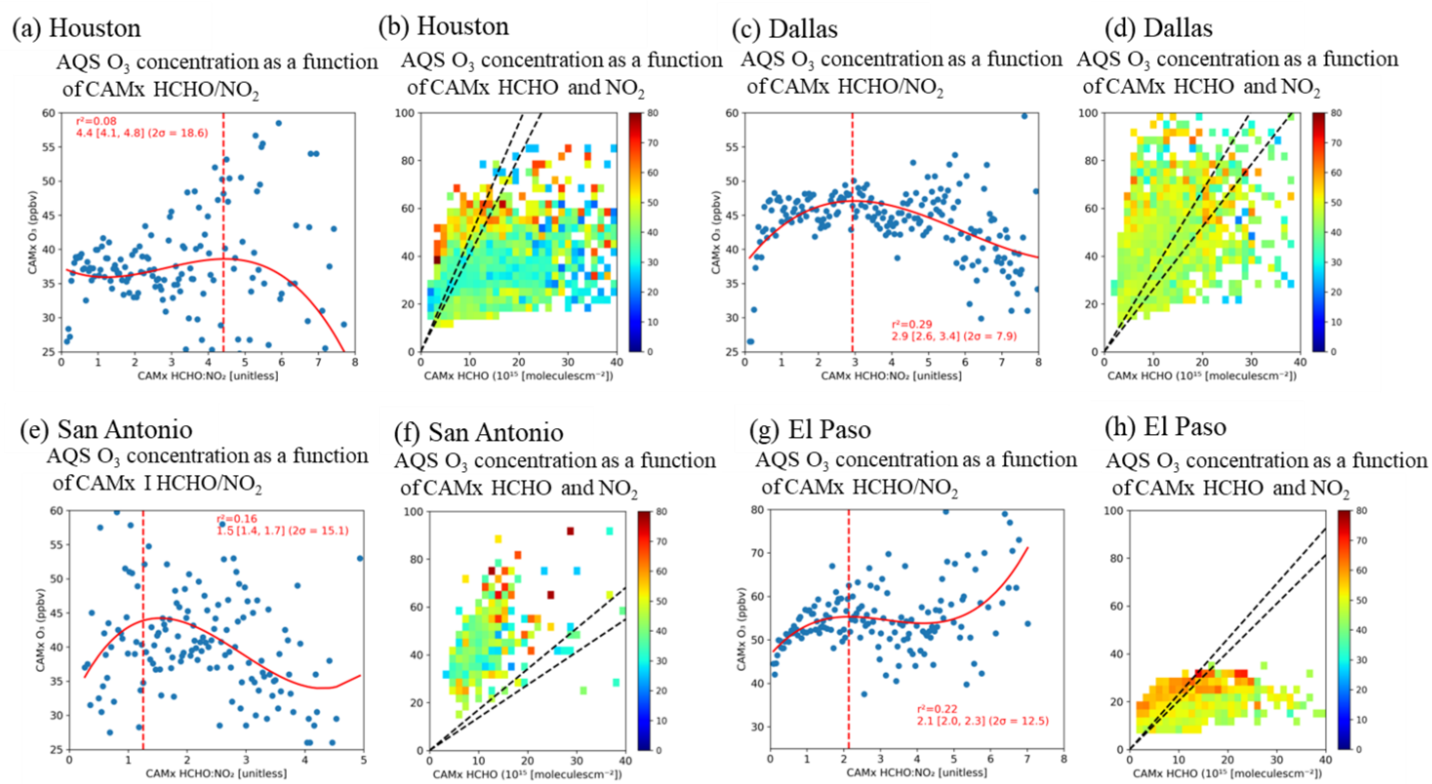

Figure 21. CAMx-derived regimes following Jin et al., 2020 methodology. Regimes in a, c, e, g are constructed by matching AQS O$_3$ concentration to its CAMx HCHO/NO$_2$ concentration. The solid lines are fitted third-order polynomial curves. The vertical dashed lines indicate the maximum of the fitted curve (labeled in the legend). The uncertainty is two standard deviations (2σ or 95% confidence interval) and the correlation coefficient is listed in the legend. AQS O$_3$ concentration as a function of CAMx HCHO and NO$_2$ in b, d, f, h. The black dashed lines delineate CAMx HCHO/NO$_2$ at the derived transitional regime listed in the legend. Please note the different y-axis scale for g.

When transition points using only CAMx products (i.e, CAMx $HCHO/NO_2$ and O_3, referred to as CAMx-CAMx) were calculated (**Figure 22**), the uncertainty decreased, shown by the high R^2 values for each urban area. CAMx-CAMx transition values for Dallas (3.2 [2.9-3.6]) and El Paso (2.6 [2.5-2.7]) compare well to values derived from oversampled TROPOMI, CAMx-AQS, and Jin et al., 2020. CAMx-CAMx values for Houston (2.9 [2.6-3.3]) and San Antonio (2.8 [2.5-3.2]) do not compare as well, where Houston CAMx-CAMx values are approximately 2x lower than oversampled TROPOMI and CAMx-AQS and San Antonio see similar discrepancies. Low transition values are likely due to similar reasons as CAMx-AQS as well as surface O_3 concentrations not reaching a similar maximum as EPA AQS observations. Using a simulated environment that provides less uncertainty, we can look into how the transition values change in different conditions and reflect local chemical and region-specific influences (**Table 6**). The total ozone season (All) and weekends see similar transition points, suggesting that the CAMx model does not capture the weekend-weekday changes as TROPOMI does (c.f. Figure 17). Compared to the total 2022 ozone season (All), the transitional value decreases in exceedances and temperatures greater than the 85th percentile. A decrease in the transition point in these conditions indicates that the airshed sees greater VOC sensitivity and suggests that O_3 production in these conditions could be controlled with limitations on VOC concentrations. Although values listed in **Table 6** are from a simulated environment, we can observe trends and apply these trends to future observations of the urban airsheds.

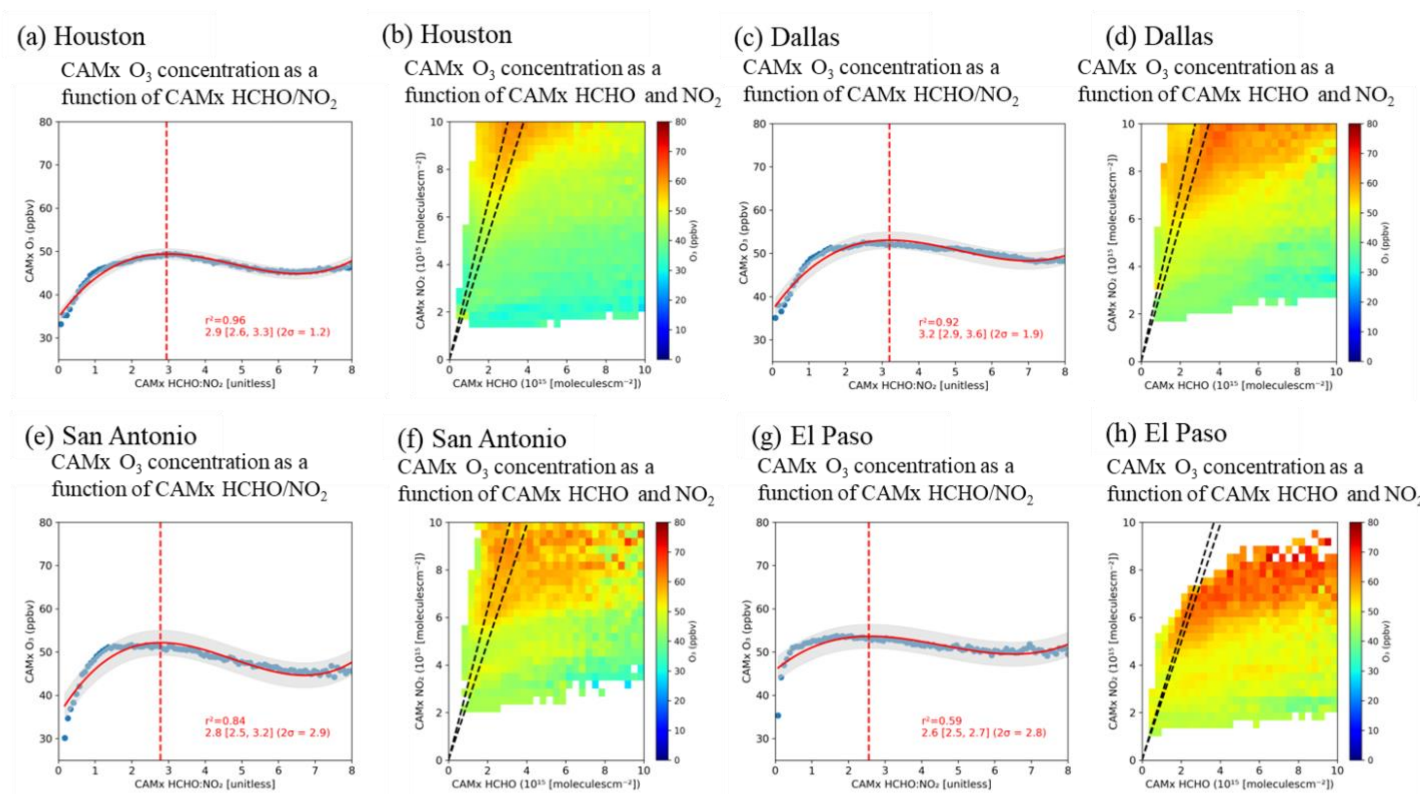

Figure 22. CAMx-derived regimes following Jin et al., 2020 methodology. Regimes in a, c, e, g are constructed by matching surface CAMx O_3 concentration to its CAMx surface $HCHO/NO_2$ concentration. The solid lines are fitted third-order polynomial curves, and the shading indicates 95% confidence intervals. The vertical dashed lines indicate the maximum of the fitted curve (labeled in the legend). The uncertainty is two standard deviations (2σ or 95% confidence interval) and the correlation coefficient is listed in the legend. CAMx O_3 concentration as a function of CAMx HCHO and NO_2 in b, d, f, h. The black dashed lines delineate CAMx $HCHO/NO_2$ at the derived transitional regime listed in the legend.

In **Figure 20**, **21**, and **22** we see that the newly derived transitional regimes for each county capture peak ozone concentrations, except for that of CAMx San Antonio (**Figure 21f**). This is consistent with the Jin et al., hypothesis that the highest O_3 concentration should be where the transitional regime occurs. Since these thresholds are calculated using in situ observations, this is more indicative of the local O_3 chemistry including the effect of NO_x titration over urban areas (Jin et al., 2020), thus this places confidence that these new regime definitions can classify an airshed as VOC-limited (O_3 production rates are limited by VOCs), NO_x-limited (O_3 production rates are limited by NO_x), and transitional (not strongly limited by VOCs or NO_x). In the updated calculation, poor agreement is still observed in oversampled TROPOMI and CAMx-AQS calculations due to the short temporal period considered (i.e., 1-5 years), relating surface O_3 concentrations to column measurements from model and satellite observations, where each data product has their own uncertainty, and similar reasons cited by Jin et al. (2020). Despite low correlation, we observe that the FNR and its transition point do change in different conditions and this change is captured by different data products. Analyzing the transition point helps to better understand the control policies that can be employed to control ozone production and protect the health of citizens across Texas urban areas.

Table 6. Transitional regimes for select conditions using surface CAMx O_3 and CAMx surface $HCHO/NO_2$ concentrations.

	Houston			Dallas			San Antonio			El Paso		
	R^2	$HCHO/NO_2$	Transitional Regime	R^2	$HCHO/NO_2$	Transitional Regime	R^2	$HCHO/NO_2$	Transitional Regime	R^2	$HCHO/NO_2$	Transitional Regime
All	0.96	2.9	2.6-3.3	0.92	3.2	2.9-3.6	0.84	2.8	2.5-3.2	0.50	2.6	2.5-2.7
Weekend	0.91	2.9	2.7-3.2	0.82	3.2	2.9-3.6	0.80	2.9	2.5-3.2	0.72	2.1	1.9-2.2
Exceedances	0.78	2.6	2.3-3.0	0.87	1.6	1.3-2.0	0.76	2.8	2.4-3.1	0.49	0.45	0.37-1.1
Temp. Greater than 85th	0.89	2.8	2.5-3.2	0.86	2.4	2.1-2.8	0.77	2.1	1.7-2.4	0.70	1.6	1.5-1.7

Table 7 lists the number of pixels changed when applying the oversampled TROPOMI-derived to the total ozone season in 2022 within each county's domain as shown in **Figure 18**. We find that with regimes derived from oversampled TROPOMI NO_2 and HCHO, surface level CAMx simulated HCHO and NO_2 produce similar regime distributions when compared to Jin et al., 2020, as indicated by the relatively low percent of grid cells changed shown in **Table 7**. Although using a simulated environment, our results show that CAMx can be used to find transition points in regions that may not be robustly sampled with extensive ground monitoring networks or field campaigns, such as other urban areas in Texas excluding Houston. We find that TROPOMI and CAMx outputs can give regime transitional points comparable to that found in the literature while being temporally updated, location-specific, and meteorologically or chemically relevant to the airshed in question.

Table 7. The number of pixels changed when applying the physical oversampled TROPOMI-derived to the total ozone season in 2022 within each county's domain as shown in **Figure 15**.

		Number of Changing Grid Cells	Number of Consistent Grid Cells	Total Grid Cells	Percent of Changing Grid Cells	Percent of Non Changing Grid Cells
	TROPOMI CAMxAMF FNR	23	2005	2028	1.13	98.87
	TROPOMI FNR	9	2019	2028	0.44	99.56
Dallas	CAMx FNR	118	1910	2028	5.82	94.18
	TROPOMI CAMxAMF FNR	998	1725	2723	36.65	63.35
	TROPOMI FNR	534	2189	2723	19.61	80.39
Houston	CAMx FNR	1427	1296	2723	52.41	47.59
	TROPOMI CAMxAMF FNR	248	113	361	68.7	31.3
	TROPOMI FNR	105	256	361	29.09	70.91
San Antonio	CAMx FNR	172	189	361	47.65	52.35
	TROPOMI CAMxAMF FNR	35	366	401	8.73	91.27
	TROPOMI FNR	21	380	401	5.24	94.76
El Paso	CAMx FNR	72	329	401	17.96	82.04

7: Limitations and Uncertainties

Utilizing TROPOMI and CAMx observations for understanding ozone sensitivity to its precursors of NO_x and VOCs is met with limitations. In this study, the O_3-NO_x-VOC relation is studied solely with $HCHO/NO_2$ and L_N/Q, and no other measurable ozone indicators such as H_2O_2 or HNO_3 were examined (Souri et al., 2023, Sillman and He, 2002). This study does not include examining the uncertainties in the deposition and effects of aerosols in O_3 sensitivity. Further, the methodology employed by Jin et al., 2020 does not consider meteorology so measured O_3 is sensitive to only its local chemical production. Additionally, it assumes that local changes in chemical or depositional loss of O_3 are insignificant on average. The empirical approach by Jin et al., 2020 are heavily affected by biases in the satellite retrieval algorithms as well as the domain selected, sampling size, and biases of both the ground-based and space-based observations (Jin et al., 2020).

Polar-orbiting instruments, like TROPOMI, have one global pass a day limiting our ability to see diurnal effects on O_3 sensitivity and constraining our understanding to the time of the overpass. When comparing TROPOMI and CAMx products in this report, only observations used at the time of TROPOMI overpass were employed. Here, we do not employ CAMx model results to explore the diurnal cycle of the FNR ratio. TROPOMI measurements occur in the early afternoon which does not capture the largest NO_x emission rates that occur in the early morning and afternoon but can capture a peak in the biogenic VOC emissions which frequently peak at the maximum daily 2m temperature, further the afternoon overpass can see a stronger photolysis rate effecting both HCHO and NO_2 (Goldberg et al., 2022). Satellite observations measure the vertically integrated column densities and density variations within the vertical column reduce the ability to resolve near-surface O_3 sensitivity (Jin et al., 2020). However, oversampling the observations using a physical-based approach from Sun et al., (2018), produces a more realistic representation of satellite observations as each field of view (FOV) is represented as a sensitivity distribution on the ground. HCHO observations see uncertainty in relation to ozone production, specifically in that the extent to which satellite-based HCHO relates to local surface organic reactivity remains unclear (Jin et al., 2020).

Uncertainties are seen with TROPOMI-derived values. The standard deviation of each derived value is listed to show the variance from the mean. Numerous studies (Goldberg et al., 2022, Souri et al., 2023, Judd et al. 2020) have illustrated low bias within the NO_2 column compared to observations from other platforms such as aircraft or ground-based spectrometer measurements. Algorithm updates have seen improvements in highly polluted or urban areas but little improvement over rural regions which could carry higher uncertainties (Eskes et al., (2023)). Nonetheless, uncertainty in the TROPOMI NO_2 column is placed around 25% following other studies (Griffin et al., 2019, Liu et al., 2022, Goldberg et al., 2019, Laughner et al., 2019). Souri et al., (2023) and De Smedt et al., (2021) observe similar errors in the HCHO column. Souri et al., (2023) shares HCHO column standard deviations of 4.32×10^{15}

molec.cm^{-2}, while De Smedt et al., (2021) report errors in the slant column density of about 6 x 10^{15} molec.cm^{-2} in remote areas. A combined uncertainty in the HCHO column is found to be 25-50% (De Smedt et al., 2018). Employing both NO_2 and HCHO TROPOMI observations creates a combined uncertainty. Souri et al., (2023) estimated that total errors in the TROPOMI FNR value range from 0-300% and that fewer errors are present in city centers, such as Houston and Dallas, compared to that of El Paso and San Antonio (see Fig. 13 in Souri et al., 2023).

Uncertainties are seen in the CAMx-derived values, whereas like with TROPOMI-derived values, the standard deviation is listed to show the variance from the mean. Uncertainties can be generated from input data, like emissions or meteorology, model parameterizations, and the formulation of physical and chemical processes in the atmosphere (Soleimanian et al., 2023). Challenges are present in modeling the atmosphere, especially in regions with complex local-scale circulations and emission profiles such as the Houston areas. A high degree of uncertainty is seen in the emission inventory with modeling simulations as this is a main driver in recreating secondary photochemical species, such as ozone (Soleimanian et al., 2023, Holnicki and Nahroski, 2015).

8: Conclusions and Recommendations

In this study, we find ground-based monitors, satellite observations, and products from the photochemical model, CAMx, can describe the ozone production regime an airshed may be in. We find that the FNR for each county of interest varies and thus a single value is not appropriate for describing an airshed across the state of Texas. Further, different conditions like weekends, weekdays, high temperatures, and O_3 exceedances exhibit different FNR values and tend towards different ozone production regimes. We conclude that for the 2022 ozone season the products used for intercomparison in this report place Houston, Dallas, San Antonio, and El Paso is different regimes considering the data product used to calculate the FNR. However, we observe that most intercomparison products place counties near their transitional regime which reflects the spatial quality of the FNR and county emissions, where areas near the main urban core are often VOC-limited while suburban or surrounding areas are NO_x-limited.

We examine the threshold defined for Houston by Jin et al. (2020) and find that it does capture FNR variations within the urban areas of Texas, specifically Houston. However, is not appropriate for use in other Texas urban areas as well as more recent observations (i.e. observations from 2016 onwards). Updated transition points were determined using oversampled TROPOMI observations and CAMx products compared to in situ ozone observations from the EPA AQS network. We place greater confidence in the oversampled TROPOMI regime thresholds due to higher agreement with fitted results as well as the method's full use of observations which are more indicative of local O_3 chemistry and its ability to resolve fine feature variability. However, this recommendation is severely limited due to the satellite-based HCHO/NO_2 transition point being limited temporally. TROPOMI cannot observe early morning hours when it is hypothesized that NO_2 emissions are at their highest diurnally, and thus we do not currently know how this would affect the FNR values across the whole ozone season. With the recent release of TEMPO NO_2 and HCHO observations (Released: May 2024 with observation starting from 8/1/2023), more robust indicator ratios can be calculated on a diurnal cycle which will give us more confidence in our understanding of the drivers of ozone production and its local chemistry in urban centers across Texas.

9: References

1. Alvarado, L. M. A., Richter, A., Vrekoussis, M., Hilboll, A., Kalisz Hedegaard, A. B., Schneising, O., and Burrows, J. P.: Unexpected long-range transport of glyoxal and formaldehyde observed from the

Copernicus Sentinel-5 Precursor satellite during the 2018 Canadian wildfires, Atmos. Chem. Phys., 20, 2057– 2072, https://doi.org/10.5194/acp-20-2057-2020, 2020.

2. Bernier, C., Y. Wang, M. Estes, R. Lei, B. Jia, S. Wang, and J. Sun: Clustering surface ozone diurnal cycles to understand the impact of circulation patterns in Houston, TX, Journal of Geophysical Research: Atmospheres, 124, 13457– 13474, https://doi.org/10.1029/2019JD031725, 2019
3. Bovensmann, H., Burrows, J. P., Buchwitz, M., Frerick, J., Noel, S., Rozanov, V. V., et al. (1999). SCIAMACHY: Mission objectives and measurement modes. Journal of the Atmospheric Sciences, 56(2), 127–150. https://doi.org/10.1175/1520-0469(1999)0562.0.co;2 Burrows, J. P., Weber, M., Buchwitz, M., Rozanov, V., Ladstatter-Weibenmayer, A., Richter, A., et al. (1999). The global ozone monitoring experiment (GOME): Mission concept and first scientific results. Journal of the Atmospheric Sciences, 56(2), 151–175. https://doi. org/10.1175/1520-0469(1999)0562.0.CO;2
4. Chen, F., Janji´c, Z., Mitchell, K., 1997. Impact of atmospheric surface-layer parameterizations in the new land-surface scheme of the NCEP mesoscale Eta model. Boundary-Layer Meteorol. 85, 391–421.
5. Chen, F., Dudhia, J., 2001. Coupling an advanced land surface–hydrology model with the Penn State–NCAR MM5 modeling system. Part I: model implementation and sensitivity. Mon. Weather Rev. 129, 569–585.
6. Choi, Y., Souri, A.H., 2015. Chemical condition and surface ozone in large cities of Texas during the last decade: observational evidence from OMI, CAMS, and model analysis. Remote Sens. Environ. 168, 90–101.
7. Copernicus Sentinel Data Processed by ESA, Koninklijk Nederlands Meteorologisch Instituut (KNMI). (2021). Sentinel-5P TROPOMI tropospheric NO_2 1-Orbit L2 5.5 km × 3.5 km. Goddard Earth Sciences Data and Information Services Center (GES DISC). https://doi.org/10.5270/S5P-9bnp8q8
8. Copernicus Sentinel data processed by ESA, German Aerospace Center (DLR) (2020), Sentinel-5P TROPOMI Tropospheric Formaldehyde HCHO 1-Orbit L2 5.5km x 3.5km, Greenbelt, MD, USA, Goddard Earth Sciences Data and Information Services Center (GES DISC), https://doi.org/10.5270/S5P-vg1i7t0
9. Demetillo, M. A. G.; Navarro, A.; Knowles, K. K.; Fields, K. P.; Geddes, J. A.; Nowlan, C. R.; Janz, S. J.; Judd, L. M.; Al-Saadi, J.; Sun, K.; McDonald, B. C.; Diskin, G. S.; Pusede, S. E. Observing nitrogen dioxide air pollution inequality using high-spatial-resolution remote sensing measurements in Houston, Texas. Environ. Sci. Technol. 2020, 54, 9882−9895.
10. De Smedt, I., Pinardi, G., Vigouroux, C., Compernolle, S., Bais, A., Benavent, N., Boersma, F., Chan, K.-L., Donner, S., Eichmann, K.-U., Hedelt, P., Hendrick, F., Irie, H., Kumar, V., Lambert, J.-C., Langerock, B., Lerot, C., Liu, C., Loyola, D., Piters, A., Richter, A., Rivera Cárdenas, C., Romahn, F., Ryan, R. G., Sinha, V., Theys, N., Vlietinck, J., Wagner, T., Wang, T., Yu, H., and Van Roozendael, M.: Comparative assessment of TROPOMI and OMI formaldehyde observations and validation against MAX-DOAS network column measurements, Atmos. Chem. Phys., 21, 12561–12593, https://doi.org/10.5194/acp-21-12561-2021, 2021.
11. De Smedt, I., Theys, N., Yu, H., Danckaert, T., Lerot, C., Compernolle, S., Van Roozendael, M., Richter, A., Hilboll, A., Peters, E., Pedergnana, M., Loyola, D., Beirle, S., Wagner, T., Eskes, H., van Geffen, J., Boersma, K. F., and Veefkind, P.: Algorithm theoretical baseline for formaldehyde retrievals from S5P TROPOMI and from the QA4ECV project, Atmos. Meas. Tech., 11, 2395– 2426, https://doi.org/10.5194/amt-11-2395-2018, 2018.
12. Dowell, D. C., and Coauthors, 2022: The High-Resolution Rapid Refresh (HRRR): An Hourly Updating Convection-Allowing Forecast Model. Part I: Motivation and System Description. Wea. Forecasting, 37, 1371–1395, https://doi.org/10.1175/WAF-D-21-0151.1.
13. Duncan, B.N., Yoshida, Y., Olson, J.R., Sillman, S., Martin, R.V., Lamsal, L., Hu, Y., Pickering, K.E., Retscher, C., Allen, D.J., Crawford, J.H., 2010. Application of OMI observations to a space-based indicator of NO_x and VOC controls on surface ozone formation. Atmos. Environ. 44 (18), 2213–2223.
14. Eskes, H. J., van Geffen, J., Boersma, F., Eichmann, K.-U., Apituley, A., Pedergnana, M., et al. (2023). Sentinel-5 precursor/TROPOMI level 2 product user manual nitrogen dioxide. Retrieved from

https://sentinel.esa.int/documents/247904/3541451/Sentinel-5P-Nitrogen-DioxideLevel-2-Product-Readme-File.%20pdf

15. Geddes, J. A.; Martin, R. V.; Boys, B. L.; van Donkelaar, A. Long-Term Trends Worldwide in Ambient NO_2 Concentrations Inferred from Satellite Observations. Environ. Health Perspect. 2016, 124 (3), 281−289.
16. Goldberg DL, Anenberg SC, Kerr GH, Mohegh A, Lu Z, Streets DG. TROPOMI NO_2 in the United States: A Detailed Look at the Annual Averages, Weekly Cycles, Effects of Temperature, and Correlation With Surface NO_2 Concentrations. Earths Future. 2021 Apr;9(4):e2020EF001665. doi: 10.1029/2020EF001665. Epub 2021 Apr 2. PMID: 33869651; PMCID: PMC8047911.
17. Goldberg, D. L., Harkey, M., de Foy, B., Judd, L., Johnson, J., Yarwood, G., and Holloway, T.: Evaluating NO_x emissions and their effect on O_3 production in Texas using TROPOMI NO_2 and HCHO, Atmos. Chem. Phys., 22, 10875–10900, https://doi.org/10.5194/acp-22-10875-2022, 2022.
18. Goldberg, D. L.; Lu, Z.; Streets, D. G.; de Foy, B.; Griffin, D.; McLinden, C. A.; Lamsal, L. N.; Krotkov, N. A.; Eskes, H. Enhanced capabilities of TROPOMI NO_2: Estimating NO_x from North American cities and power plants. Environ. Sci. Technol. 2019, 53, 12594−12601.
19. Goldberg, D. L., Lamsal, L. N., Loughner, C. P., Swartz, W. H., Lu, Z., and Streets, D. G.: A high-resolution and observationally constrained OMI NO_2 satellite retrieval, Atmos. Chem. Phys., 17, 11403–11421, https://doi.org/10.5194/acp-17-11403-2017, 2017.
20. Griffin, D., Zhao, X., McLinden, C. A., Boersma, F., Bourassa, A., Dammers, E., Degenstein, D., Eskes, H., Fehr, L., Fioletov, V., Hayden, K., Kharol, S. K., Li, S., Makar, P., Martin, R.V., Mihele, C., Mittermeier, R.L., Krotkov, N., Sneep, M., Lamsal, L.N., et al. (2019). High-resolution mapping of nitrogen dioxide with TROPOMI: First results and validation over the Canadian oil sands. Geophysical Research Letters, 46, 1049– 1060. https://doi.org/10.1029/2018GL081095.
21. He, H., Hembeck, L., Hosley, K. M., Canty, T. P., Salawitch, R. J., & Dickerson, R. R. (2013). High ozone concentrations on hot days: The role of electric power demand and NO_x emissions. *Geophysical Research Letters*, **40**(19), 5291–5294. https://doi.org/10.1002/grl.50967
22. Holnicki, P., Nahorski, Z., 2015. Emission data uncertainty in urban air quality modeling—case study. Environ. Model. Assess. 20, 583–597.
23. Iacono, M.J., Delamere, J.S., Mlawer, E.J., Shephard, M.W., Clough, S.A., Collins, W.D., 2008. Radiative forcing by long-lived greenhouse gases: calculations with the AER radiative transfer models. J. Geophys. Res. Atmos. 113.
24. Jeon, W., Choi, Y., Souri, A.H., Roy, A., Diao, L., Pan, S., Lee, H.W., Lee, S.H., 2018. Identification of chemical fingerprints in long-range transport of burning induced upper tropospheric ozone from Colorado to the North Atlantic Ocean. Sci. Total Environ. 613, 820–828.
25. Jin, X., Fiore, A. M., Boersma, K. F., De Smedt, I., and Valin, L. (2020): Inferring changes in summertime surface ozone-NO_x-VOC chemistry over U.S. urban areas from two decades of satellite and ground-based observations, Environ. Sci. Technol., 54, 6518– 6529, https://doi.org/10.1021/acs.est.9b07785.
26. Jin, X., Fiore, A. M., Murray, L. T., Valin, L. C., Lamsal, L. N., Duncan, B., et al. (2017). Evaluating a space-based indicator of surface ozone-NO_x-VOC sensitivity over midlatitude source regions and application to decadal trends. Journal of Geophysical Research: Atmospheres, 122(19), 10439–10461. https://doi.org/10.1002/2017JD026720
27. Jin, X., & Holloway, T. (2015). Spatial and temporal variability of ozone sensitivity over China observed from the Ozone Monitoring Instrument. Journal of Geophysical Research: Atmospheres, 120(14), 7229–7246. https://doi.org/10.1002/2015JD023250
28. Johnson, M. S., Philip, S., Meech, S., Kumar, R., Sorek-Hamer, M., and Shiga, Y. P.: Insights into the long-term (2005–2021) spatiotemporal evolution of summer ozone production sensitivity in the Northern Hemisphere derived with OMI, EGUsphere [preprint], https://doi.org/10.5194/egusphere-2024-583, 2024. [preprint]
29. Judd, L. M., Al-Saadi, J. A., Szykman, J. J., Valin, L. C., Janz, S. J., Kowalewski, M. G., Eskes, H. J., Veefkind, J. P., Cede, A., Mueller, M., Gebetsberger, M., Swap, R., Pierce, R. B., Nowlan, C. R., Abad,

G. G., Nehrir, A., and Williams, D.: Evaluating Sentinel-5P TROPOMI tropospheric NO_2 column densities with airborne and Pandora spectrometers near New York City and Long Island Sound, Atmos. Meas. Tech., 13, 6113–6140, https://doi.org/10.5194/amt-13-6113-2020, 2020.
30. Kleipool, Q. L., Dobber, M. R., de Haan, J. F., and Levelt, P. F.: Earth surface reflectance climatology from 3 years of OMI data, J. Geophys. Res.-Atmos., 113, 1–22, https://doi.org/10.1029/2008JD010290, 2008.
31. Kleinman, L.I., 2005. The dependence of tropospheric ozone production rate on ozone precursors. Atmos. Environ. 39, 575–586.
32. Kleinman, L.I., Daum, P.H., Lee, Y., Nunnermacker, L.J., Springston, S.R., Weinstein-Lloyd, J., Rudolph, J., 2001. Sensitivity of ozone production rate to ozone precursors. Geophys. Res. Lett. 28, 2903–2906.
33. Kleinman, L.I., Daum, P.H., Imre, D., Lee, Y., Nunnermacker, L.J., Springston, S.R., Weinstein-Lloyd, J., Rudolph, J., 2002. Ozone production rate and hydrocarbon reactivity in 5 urban areas: a cause of high ozone concentration in Houston. Geophys. Res. Lett. 29, 101–105.
34. Kleinman, L.I., Daum, P.H., Lee, Y., Nunnermacker, L.J., Springston, S.R., Weinstein-Lloyd, J., Rudolph, J., 2005. A comparative study of ozone production in five US metropolitan areas. J. Geophys. Res. Atmos. 110.
35. Kleinman, L. I., Daum, P. H., Imre, D. G., Lee, J. H., Lee, Y. N., Nunnermacker, L. J., et al. (2000). Ozone production in the New York City urban plume. Journal of Geophysical Research Atmospheres, 105(D11), 14495–14511. https://doi.org/10.1029/2000JD900011
36. Laughner, J. L.; Cohen, R. C. Direct observation of changing NO_x lifetime in North American cities. Science 2019, 366, 723−727.
37. Lee, T., & Wang, Y. (2023). CLASP: CLustering of Atmospheric Satellite Products and its applications in feature detection of atmospheric trace gases. Journal of Geophysical Research: Atmospheres, 128, e2023JD038887. https://doi.org/10.1029/2023JD038887
38. Lee, T., Wang, Y., & Sun, K. (2022). Impact of Hurricane Ida on nitrogen oxide emissions in southwestern Louisiana detected from space. Environmental Science and Technology Letters, 9(10), 808–814. https://doi.org/10.1021/acs.estlett.2c00414
39. Levelt, P. F., van den Oord, G. H. J., Dobber, M. R., Malkki, A., Huib Visser, A., Johan de Vries, H., et al. (2006). The ozone monitoring instrument. IEEE Transactions on Geoscience and Remote Sensing, 44(5), 1093–1101. https://doi.org/10.1109/TGRS.2006.872333
40. Li, W., Y. Wang, Bernier, C., & Estes, M.: Identification of sea breeze recirculation and its effects on ozone in Houston, TX, during DISCOVER-AQ 2013. Journal of Geophysical Research: Atmospheres, 125, https://doi.org/10.1029/2020JD033165, 2020
41. Li, W., Wang, Y., Liu, X., Soleimanian, E., Griggs, T., Flynn, J., Walter, P., 2023. Understanding offshore high-ozone events during TRACER-AQ 2021 in Houston: insights from WRR-CAMx photochemical modeling. Egusph. https://doi.org/ 10.5194/egusphere-2023-1117.
42. Liu, F.; Tao, Z.; Beirle, S.; Joiner, J.; Yoshida, Y.; Smith, S. J.; Knowland, K. E.; Wagner, T. A new method for inferring city emissions and lifetimes of nitrogen oxides from high-resolution nitrogen dioxide observations: a model study. Atmos. Chem. Phys. 2022, 22, 1333−1349.
43. Martin, R. V., Fiore, A. M., & Van Donkelaar, A. (2004). Space-based diagnosis of surface ozone sensitivity to anthropogenic emissions. Geophysical Research Letters, 31(6). https://doi.org/10.1029/2004GL019416
44. Mazzuca, G. M., Ren, X., Loughner, C. P., Estes, M., Crawford, J. H., Pickering, K. E., et al. (2016). Ozone production and its sensitivity to NO_x and VOCs: Results from the DISCOVER-AQ field experiment, Houston 2013. Atmospheric Chemistry and Physics, 16(22), 14463–14474. https://doi.org/10.5194/acp-16-14463-2016
45. Morrison, H., Thompson, G., Tatarskii, V., 2009. Impact of cloud microphysics on the development of trailing stratiform precipitation in a simulated squall line: comparison of one-and two-moment schemes. Mon. Weather Rev. 137, 991–1007.

46. Nakanishi, M., Niino, H., 2009. Development of an improved turbulence closure model for the atmospheric boundary layer. J. Meteorol. Soc. Japan. Ser. II 87, 895–912.
47. Pusede, S. E.; Cohen, R. C. On the Observed Response of Ozone to NO_x and VOC Reactivity Reductions in San Joaquin Valley California 1995−Present. Atmos. Chem. Phys. 2012, 12 (18), 8323−8339.
48. Schroeder, J.R., Crawford, J.H., Fried, A., Walega, J., Weinheimer, A., Wisthaler, A., Müller, M., Mikoviny, T., Chen, G., Shook, M., Blake, D.R., 2017. New insights into the column CH2O/NO_2 ratio as an indicator of near-surface ozone sensitivity. J. Geophys. Res.: Atmospheres 122 (16), 8885–8907.
49. Sillman, S. and He, D.: Some theoretical results concerning O3- NO_x -VOC chemistry and NO_x -VOC indicators, J. Geophys. Res., 107, 4659, https://doi.org/10.1029/2001JD001123, 2002.
50. Soleimanian, E., Y. Wang, W. Li, X. Liu, T. Griggs, J. Flynn, P. J. Walter, and M. J. Estes, 2023: Understanding ozone episodes during the TRACER-AQ campaign in Houston, Texas: The role of transport and ozone production sensitivity to precursors. Sci. Total Environ., 900, 165881, https://doi.org/10.1016/ j.scitotenv.2023.165881.
51. Souri, A. H., Johnson, M. S., Wolfe, G. M., Crawford, J. H., Fried, A., Wisthaler, A., Brune, W. H., Blake, D. R., Weinheimer, A. J., Verhoelst, T., Compernolle, S., Pinardi, G., Vigouroux, C., Langerock, B., Choi, S., Lamsal, L., Zhu, L., Sun, S., Cohen, R. C., Min, K.-E., Cho, C., Philip, S., Liu, X., and Chance, K.: Characterization of errors in satellite-based HCHO ⁄ NO_2 tropospheric column ratios with respect to chemistry, column-to-PBL translation, spatial representation, and retrieval uncertainties, Atmos. Chem. Phys., 23, 1963–1986, https://doi.org/10.5194/acp-23-1963-2023, 2023.
52. Souri, A. H., Nowlan, C. R., Wolfe, G. M., Lamsal, L. N., Chan Miller, C. E., Abad, G. G., et al. (2020). Revisiting the effectiveness of HCHO/ NO_2 ratios for inferring ozone sensitivity to its precursors using high resolution airborne remote sensing observations in a high ozone episode during the KORUS-AQ campaign. Atmospheric Environment, 224, 117341. https://doi.org/10.1016/j.atmosenv.2020.117341
53. Sun, K., Zhu, L., Cady-Pereira, K., Chan Miller, C., Chance, K., Clarisse, L., Coheur, P. F., González Abad, G., Huang, G., Liu, X., van Damme, M., Yang, K., & Zondlo, M. (2018). A physics-based approach to oversample multi-satellite, multispecies observations to a common grid. Atmospheric Measurement Techniques, 11(12), 6679–6701. https://doi.org/10.5194/amt-11-6679-2018.
54. Tiedtke, M., 1989. A comprehensive mass flux scheme for cumulus parameterization in large-scale models. Mon. Weather Rev. 117, 1779–1800.
55. Theys, N., Volkamer, R., Müller, J. F., Zarzana, K. J., Kille, N., Clarisse, L., De Smedt, I., Lerot, C., Finkenzeller, H., Hendrick, F., Koenig, T. K., Lee, C. F., Knote, C., Yu, H., and Van Roozendael, M.: Global nitrous acid emissions and levels of regional oxidants enhanced by wildfires, Nat. Geosci., 13, 681– 686, https://doi.org/10.1038/s41561-020-0637-7, 2020.
56. Veefkind, J. P., Aben, I., McMullan, K., Förster, H., de Vries, J., Otter, G., et al. (2012). TROPOMI on the ESA sentinel-5 precursor: A GMES mission for global observations of the atmospheric composition for climate, air quality and ozone layer applications. Remote Sensing of Environment, 120, 70–83. https://doi.org/10.1016/j.rse.2011.09.027
57. Williams, J. E., Folkert Boersma, K., Le Sager, P., and Verstraeten, W. W.: The high-resolution version of TM5-MP for optimized satellite retrievals: Description and validation, Geosci. Model Dev., 10, 721–750, https://doi.org/10.5194/gmd-10-721- 2017, 2017.
58. Wolfe, G. M., Kaiser, J., Hanisco, T. F., Keutsch, F. N., De Gouw, J. A., Gilman, J. B., et al. (2016). Formaldehyde production from isoprene oxidation across NO_x regimes. Atmospheric Chemistry and Physics, 16(4), 2597–2610. https://doi.org/10.5194/acp-16- 2597-2016
59. Wu, W., Fu, T., Arnold, S., Spracklen, D., Zhang, A., Tao, W., Wang, X., Hou, Y., et al., (2024). Temperature-Dependent Evaporative Anthropogenic VOC Emissions Significantly Exacerbate Regional Ozone Pollution. Environmental Science & Technology, 58 (12), 5430-544, DOI: 10.1021/acs.est.3c09122.
60. Xiong, Y., Chai, J., Mao, H., Mariscal, N., Yacovitch, T., Lerner, B., et al. (2023). Examining the summertime ozone formation regime in Southeast Michigan using MOOSE ground-based HCHO/ NO_2

measurements and F0AM box model. Journal of Geophysical Research: Atmospheres, 128, e2023JD038943. https://doi.org/10.1029/2023JD038943
61. Zhang, C., Wang, Y., Hamilton, K., 2011. Improved representation of boundary layer clouds over the southeast Pacific in ARW-WRF using a modified Tiedtke cumulus parameterization scheme. Mon. Weather Rev. 139, 3489–3513.
62. Sax, Sonja, et al. How Ozone Pollution Affects Public Health in San Antonio: An Analysis Commissioned by the City of San Antonio, Sept. 2017, www.sanantonio.gov/Portals/0/Files/Sustainability/OzoneHealth/final-report.pdf.

10: Appendix

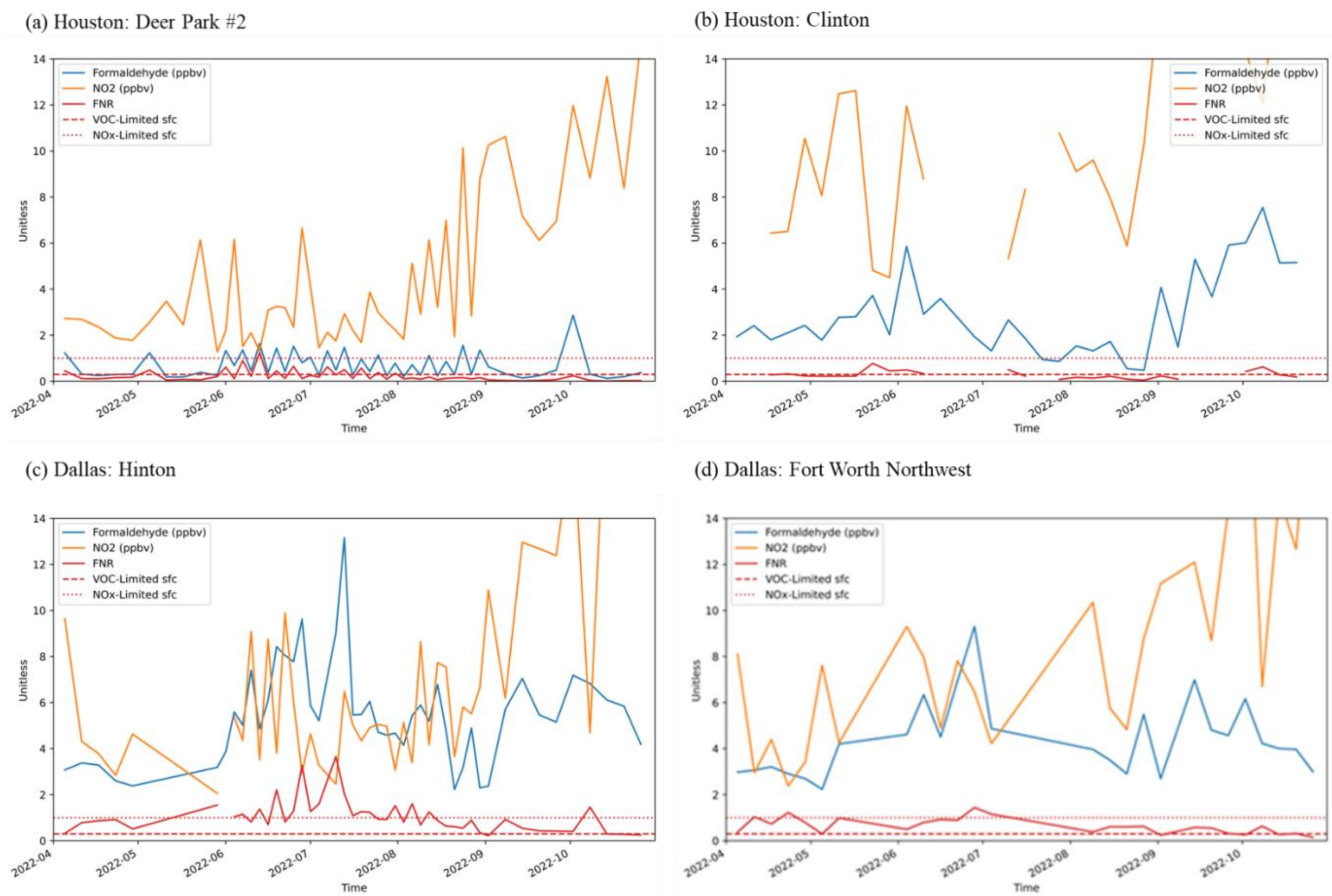

Figure 1. Timeseries of formaldehyde (blue), nitrogen dioxide (orange) and FNR (red) 2022 for the site (a) Deer Park #2 and (b) Clinton in the region Houston, TX, and (c) Hinton, and (d) Fort Worth Northwest in the region Dallas, TX. Transitional regimes follow from Blanchard (2020).